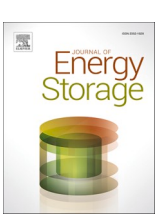
ELSEVIER

Contents lists available at ScienceDirect

Journal of Energy Storage

journal homepage: www.elsevier.com/locate/est



Research papers

Novel latent heat storage via volumetric radiation and nanofluid natural convection: A Lattice Boltzmann study

Hashem Ahmadi Tighchi ^{a,b}, Masoud Sobhani ^a, Javad Abolfazli Esfahani ^{a,c,*}

- a Department of Mechanical Engineering, Faculty of Engineering, Ferdowsi University of Mashhad, Mashhad, Iran
- ^b Sustainable Thermal Technology Research Core, Ferdowsi University of Mashhad, Mashhad, Iran
- ^c Engineering College, Lishui University, Lishui, China

ARTICLE INFO

Keywords: PCM block Volumetric radiation Natural convection Nanofluid Radiative properties Heat storage LBM

ABSTRACT

This paper presents numerical simulation of the heat storage problem via a conductive block containing a phase change material (PCM) placed inside a nanofluid. Energy storage during combined heat transfer using PCMs is a critical issue in modern thermal systems. In this research, natural convection and radiation mechanisms are examined inside the two-dimensional medium filled with water-Al2O3 nanofluid by considering the real radiation properties of nanoparticles in the governing equations. The radiation presence is assumed in the participating medium to investigate its effects on the temperature distribution and phase change propagation. Numerical calculations are carried out utilizing the full lattice Boltzmann method (LBM). The variation of parameters such as the Planck number, Rayleigh number, block size and nanofluid concentration is studied. The results show that volumetric radiation can enhance the phase change by >50 % compared to pure natural convection. However, the radiation effects decrease with increasing Planck number and block size. Moreover, increasing the nanofluid concentration from 0.1 % to 0.3 % reduces the liquid fraction by up to 5.5 % due to its absorbing and scattering properties. The findings confirm that LBM simulation can reveal the influences of integrating volumetric radiation into PCM block-nanofluid systems, providing applicable insights for the design of energy storage and thermal management systems.

1. Introduction

Thermal energy storage and thermal management are topics of interest in many thermal engineering systems such as solar power, batteries, equipment cooling and air conditioning. Critical factors such as cost and environmental issues should be considered in the efficient design of these systems. One of the most appropriate methods to improve energy management in thermal systems is the use of phase change materials (PCMs). These materials benefit from the advantages of storing and releasing large amounts of energy during phase change.

Therefore, it has caused them to be proposed as energy storage. Desirable characteristics such as high energy density, suitable melting temperature for the intended application, high latent heat, properties stability, and reasonable cost have increased the tendency to use phase change materials. Over the past decade, there has been a notable increase in research publications focusing on PCMs for engineering applications including solar energy storage, electronic cooling, air conditioning, batteries etc. [1–3].

In previous investigations, heat transfer examination in the presence of a PCM block has always been the main focus of researchers due to its high compatibility with the practical concerns of energy systems. Selimefendigil and coworkers [4] investigated natural convection in a two-dimensional cavity filled with a nanofluid and a PCM block. A conductive partition was attached to the right wall in the presence of an inclined magnetic force. It was found that the increasing of thermal conductivity ratio and decreasing the height of the PCM block improved average and local heat transfer.

Boujelbene et al. [5] numerically examined the thermal behavior of an inclined heat sink by considering metal fins placed into PCM to improve thermal conductivity. This study showed that tree-shaped fins can create temperature uniformity in the heat sink. Also, the melting rate for fins with different shapes depends on the inclination angle of the device. Oztop et al. [6] analyzed the opening parameters effects on the natural convection in a partially open enclosure during melting of the PCM block inserted into it. Also, the bottom wall is covered by a finned heater. It was observed that a fully open cavity notably influences the dynamic of phase change while this effect reduces for a cavity with a

^{*} Corresponding author at: Department of Mechanical Engineering, Faculty of Engineering, Ferdowsi University of Mashhad, Mashhad, Iran. E-mail address: Abolfazl@um.ac.ir (J. Abolfazli Esfahani).

Nome	nclature	\overrightarrow{u}	macroscopic velocity vector
		U, V	dimensionless velocity components
c	speed of light	w	weight
C	lattice speed	w_g	radiative weight
C_s	speed of sound	x, y	<i>x</i> - and <i>y</i> -coordinate system
C_p	specific heat	X, Y	dimensionless coordinate of the 2D rectangular enclosure
Ď	nanoparticle diameter	,	<i>Q</i>
En	local enthalpy	Greek s	symbols
\overrightarrow{e}_i	velocity in discrete direction <i>i</i>	α	thermal diffusion
f_l	liquid fraction	β	extinction coefficient
fi	particle distribution function for velocity field	eta_t	coefficient of thermal expansion
-	1	γ	polar angle
$f_i^{(eq)}$	equilibrium distribution function for velocity field	δ	azimuthal angel
g_i	particle distribution function for thermal field	ε	emissivity of radiative wall
$g_i^{(eq)}$	equilibrium distributionfunction for thermal field	θ	dimensionless temperature
g_y	gravitational acceleration	κ_a	absorption coefficient
Fo	Fourier number	κ	complex component of the refractive index
G	incident radiation	ν	kinematic viscosity
Н	height and width of enclosure	ρ	density
I	intensity	σ	Stefan-Boltzmann constant
I_b	black body intensity, $\sigma T^4/\pi$	σ_{s}	scattering coefficient
I_i	particle distribution function for radiative heat transfer	ϕ	volume fraction
	-	•	size factor
$I_i^{(eq)}$	equilibrium distribution function for radiative heat	χ λ	wave length
	transfer		dynamic viscosity
J_i	buoyant body force term	μ	relaxation time for radiation
k	thermal conductivity	$ au_i$	relaxation time for thermal field
1	height and width of PCM block	$ au_t$	relaxation time for velocity field
L_f	latent heat	$ au_{ u}$	•
Ма	Mach number	ω	scattering albedo
m	relative refractive index	Ω	direction, (γ, δ)
N	refractive index	$\Delta\Omega$	solid angel, $sin\gamma d\gamma d\delta$
\overrightarrow{n}	outer normal unit vector	Δt	time step
Nu	Nusselt number	Δx	space step
P	scattering phase function	Subscri	ints
Pl	plank number	b	black
Pr	Prandtl number	C	cold
Q_{abs}	absorption efficiency	f	fluid
Q _{ext}	extinction efficiency	J H	hot
Q_{abs}	scattering efficiency	i	index for the discrete direction
	radiative heat flux		
\overrightarrow{q}_R		m C	melting point
R	ideal gas constant	nf	nanofluid
Ra	Rayleigh number	p	particle
R_k	ratio of thermal conductivity	S	solid phase
\overrightarrow{r}	position vector	W	wall
S	geometric distance	У	y-direction
t	time	Sunarca	crints
St	Stefan number	Superso	equilibrium
T	temperature	(eq)	equinorium

partially open geometry.

A numerical study about storing of thermal energy from a fined heater using various PCMs in a rectangular close medium was conducted by Oztop and coworkers [7]. The effects of physical and geometrical parameters were studied and the results indicated that different types of PCM can significantly change the total melting time, consequently, performance of the system. Bondareva and Shermet [8] analyzed the heat transfer of a wall with a multi-PCM block to build a renewable energy consuming system. The effects of different PCMs and locations were explored. The finding showed that a higher number of PCM blocks with fixed volume decreases the time of the phase transition process. Boujalbaneh et al. [9] studied PCMs in a vertical cavity with solid fins and differential heating, assuming non-Newtonian fluid flow. They

found that increasing the number of solid fins significantly reduced the melting time and improved the phase change process near the fins.

Oztop et al. [10] numerically investigated the melting and natural convection of two nanofluids in a divided domain with nano-enhanced PCMs block. The nanoparticle volume fraction and a Grashof number were considered to control flow and thermal fields. It was concluded that the thermal gradient in the domain affects the melting layer thickness and a higher Grashof number is better for improving thermal energy storage.

Researchers have always been looking for ways to improve heat transfer in the thermal storage problem with and without PCM blocks in the working fluid. One of the ways to increase heat transfer and improve the performance of energy storage systems is to use nanoparticles. For

this purpose, nanofluids were introduced, which are created by adding a certain amount of nanoparticles to a base fluid [11,12]. Adding nanoparticles to the base fluid alters its thermophysical properties, leading to modifications in fluid flow characteristics. For example, the presence of nanoparticles increases the effective viscosity and thermal conductivity, which can affect convective flow at higher concentrations.

Moreover, the optical properties of nanoparticles influence the way radiation interacts with the fluid and subsequently changes the convective flow structures [13,14]. Consequently, nanofluids create a coupled radiative-convective system that differs fundamentally from conventional pure fluids in terms of both flow patterns and thermal behavior. Therefore, many studies have been conducted on the nanofluid effects in energy management and engineering applications [13,15]. It should be noted that in most of these studies, radiative transfer has been omitted or approximations such as the Roseland model have been used for its effect. So, the results are inconsistent with the real conditions and it may cause errors in the analysis.

Furthermore, the natural convection heat transfer of laminar flow is usually low, so radiative heat transfer can be compared to this mechanism even at moderate temperatures (i.e., in the melting temperature range of PCMs). On the other hand, nanoparticles have optical properties that absorb, emit, and scatter radiation waves. Accordingly, nanofluids create a radiation-participating media that should be considered in numerical investigations.

Numerical simulations of volumetric radiation have always faced various issues due to their high complexity and considering a spherical space, which has caused the solution time to increase significantly. In the last decade, Mishra et al. [16-18] presented the Lattice Boltzmann method (LBM) to solve the radiation transfer equation (RTE) in the medium that absorbs, emits and scatters thermal radiation. The results reported in the previous articles showed that this method can provide accurate results in solving the radiation equation and also reduce the calculation time noticeably.

The LBM has other advantages including the ability to solve fluid flow and heat transfer equations and simplicity in programming. Ahmadi Tighchi et al. [19–21] utilized the LBM to simulate the combined problem of natural convection and volumetric radiation in two-dimensional enclosures and showed that this method has a suitable ability to solve the coupled equations of flow, temperature and radiation. Also, Esfahani and coworkers [22,23] used this method for the first time to solve convection heat transfer and volumetric radiation considering the real optical properties of nanoparticles and reported novel results. This method is still of interest in recent years so researchers have solved the RTE coupled with other equations using the LBM and have presented the analysis of various physical domains [24,25].

Despite extensive research on PCM block-based energy storage systems, the role of volumetric radiation in nanoparticle-enhanced heat transfer processes remains underexplored. Therefore, this research focused for the first time on the thermal energy storage system of PCM blocks with regard to volumetric radiation and natural convection considering the impacts of the absorbing, scattering and emitting properties of nanofluids. This study pioneers the use of a robust full LBM to solve all the governing equations of the considered system, including RTE. Consequently, both the upcoming issues, i.e. Roseland approximation errors and the time-consuming nature of complex numerical methods, will be resolved. The results include radiation presence, Planck number variations, block size, and nanofluid concentration effects that can be used in the engineering design of energy storage and thermal management systems that utilize nanofluids and PCM blocks.

2. Problem statement

One of the applications of phase change materials is to use them in solar systems as energy storage. In these systems, with the use of PCMs, not only energy is stored during the day, but also the excessive increase in temperature is prevented, and then the stored energy is used during the night when the outside air is cooler. The considered system has a heat absorbing part assuming a high temperature on the inner surface and a cold surface with a low temperature for heat transfer to a cold space and the rest of the surfaces are insulated. The PCM block is located in the center of the system, around which nanofluid is used to improve heat transfer. The conjugate of natural convection and radiative heat transfer in nanofluid media with conducting PCM block is occurred during heat transfer from the hot wall to the cold wall. There is no heat dissipation/generation within the medium and PCM blocks. A schematic of the intended system is shown in Fig. 1(a).

Therefore, the physical model discussed in this research is a two-dimensional enclosure, with a hot boundary of constant temperature $T_{\rm H}$ and a cold boundary of constant temperature $T_{\rm C}$, and the horizontal boundaries are insulated. The PCM block has a length of X_b and a width of Y_b , $(X_b=Y_b=l).$ The phase change material is considered to be paraffin, whose melting temperature is within the working temperature range of solar systems.

The thermophysical properties of paraffin are tabulated in Table 1, which was previously presented in reference [26]. Around the PCM block is water-Al $_2$ O $_3$ nanofluid. The average nanoparticle diameter of spherical shape Al $_2$ O $_3$ powders is 13 nm, based on previous literature on nanofluid radiative properties [27]. The aggregation of nanoparticles is neglected due to the dilute nature of the considered nanofluid.

For the nanofluid, natural convection and volumetric radiation heat transfer are taken into account by considering the constant thermophysical properties of nanofluid, except for density to perform the buoyancy force. The fluid flow is formed by the density changes due to the temperature difference, which is modelled using the Boussinesq approximation. The incompressible, laminar and Newtonian fluid flow in the system is assumed. Phase change and conduction are also dominant in the PCM block. All enclosure surfaces and PCM block walls are considered diffused and gray with constant emission. The nanofluid is considered a homogeneous and radiative participating medium, where the real optical properties of nanoparticles are used from experimental results in solving the radiation equation.

Effects of incorporating volumetric radiation, dimensions of PCM block, Rayleigh number, Ra, Planck number, Pl, and concentration of nanofluid, φ , on the heat transfer and phase change rate of PCM block are discussed. The default values of the non-dimensional numbers and parameters are based on previous studies and practical thermal energy storage applications such as [22,28].

3. Mathematical formulation/mathematical modelling

3.1. Radiative properties for nanofluid

The nanofluid optical properties including the scattering and extinction efficiencies are determined using the Rayleigh theory. These properties are significant parameters in the heat transfer simulation of a fluid zone considering the volumetric radiation. It is worth mentioning that these optical properties of nanoparticles should be controlled in a way that is in line with the application of nanofluids in the thermal system. The absorption and scattering coefficients of Al₂O₃ nanofluid have been examined in previous studies such as [29,30]. It was found that the radiation absorption property of the Al₂O₃ nanofluid could be the highest in a certain concentration of nanoparticles. In the following, a brief description of Rayleigh's theory is presented for estimating optical properties.

One of the imperative parameters in Rayleigh theory to find radiation properties is the dimensionless particle size χ . It is defined as follows [31,32]:

$$\chi = \frac{\pi D}{\lambda} \tag{1}$$

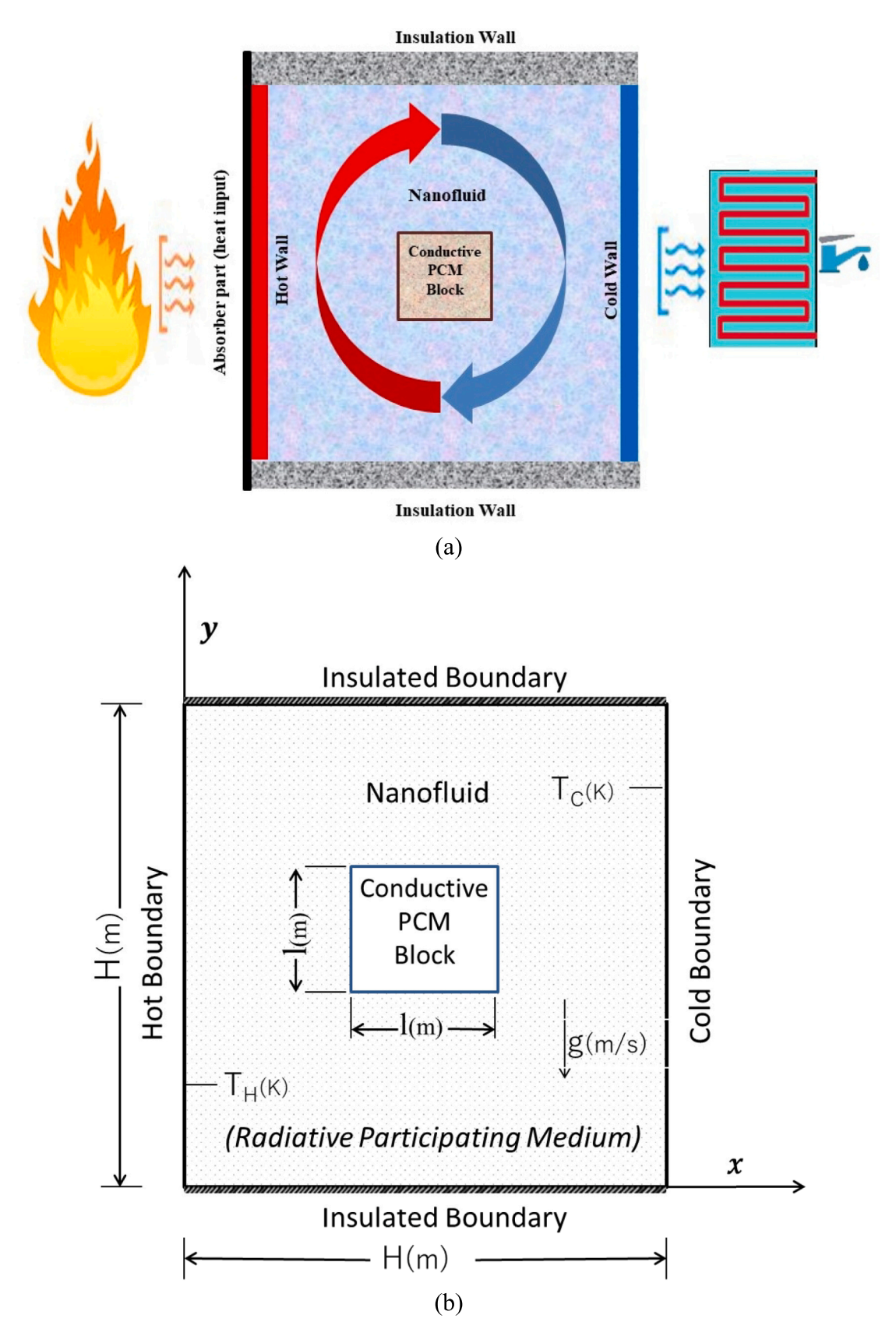


Fig. 1. (a) A schematic of the desired problem of heat storage and transfer. (b) The coordinate system and schematic diagram of the problem.

Table 1Thermophysical properties of paraffin.

	C_p (J/Kg.K)	$\rho \left({\rm Kg/m^3} \right)$	k (W/m.K)	Tm (C)	$L_{\rm f}~({\rm KJ/kg})$
Values	2412	804	0.148	50	184,480

where, λ and D are the wavelength of incident light and the nanoparticle diameter, respectively. The Rayleigh equations to determine nanoparticle efficiencies of scattering and absorbing properties are defined as follows [31,32]:

$$Q_{scat} = \frac{8}{3} \chi^4 \left| \frac{m^2 - 1}{m^2 + 2} \right|^2 \tag{2}$$

$$Q_{abs} = 4\chi Im \left\{ \frac{m^2 - 1}{m^2 + 2} \left[1 + \frac{\chi^2}{15} \left(\frac{m^2 - 1}{m^2 + 2} \right) \times \frac{m^4 + 27m^2 + 38}{2m^2 + 3} \right] \right\}$$
 (3)

where the relative refractive index m due to nanoparticles immersing in the fluid is calculated using the refractive index N by the following relationship [31,32]:

$$m = \frac{N_p}{N_\ell} \tag{4}$$

where N_p and N_f are the refractive index of particle and fluid, respectively. The extinction efficiency defines the total values of scattering and absorbing efficiencies as follows [31,32]

$$Q_{ext} = Q_{abs} + Q_{scat} (5)$$

Accordingly, the extinction coefficient is represented by

$$\beta = \kappa_a + \sigma_s \tag{6}$$

where κ_a and σ_s denote the absorbing and scattering coefficients, respectively. For a monodisperse media, the extinction coefficient can be calculated by the obtained data of the single particle [31,32]

$$\beta_p = \frac{3}{2} \frac{\phi(Q_{ext})}{D} \tag{7}$$

Additionally, for the base fluid, the extinction coefficient is estimated as follows:

$$\beta_f = \frac{4\pi\kappa_f}{\lambda} \tag{8}$$

where κ_f indicates the base fluid complex component of the refractive index. Consequently, the extinction coefficient of nanofluid is computed as

$$\beta_{nf} = \beta_p + \beta_f \tag{9}$$

According to the mentioned relationships and using the data presented in the literature [27], general radiation properties of nanofluid are provided in Table 2.

3.2. Models for the nanofluid thermophysical properties

The thermophysical properties of a fluid change due to the presence of nanoparticles. So, models must be provided to use in the simulation of nanofluid flow and heat transfer. These properties are usually estimated by correlations of pure properties and concentration. Table 3 presents

Table 2Radiative properties of Al₂O₃ nanofluid.

Volume fraction	$\sigma_s \left(\mathbf{m}^{-1} \right)$	$\beta \left(\mathbf{m}^{-1} \right)$
$\phi = 0.1\%$	2.3	16.5
$\phi = 0.3\%$	6.8	20

 Table 3

 Water and nanoparticles thermophysical properties.

	$C_p (J/Kg.K)$	$\rho \left({\rm Kg}/{\rm m}^3 \right)$	$k (\mathrm{W/m.K})$	$\mu~({\rm Pa.s})$	$\beta_t \ (1/\mathrm{K})$
Pure water	4179	997.1	0.613	8.91×10^{-4}	21×10^{-5}
Al_2O_3	765	3970	40	-	$\begin{array}{l} 0.85 \times \\ 10^{-5} \end{array}$

the properties of base fluid and nanoparticles from [33,34], which are water and Al_2O_3 , respectively.

Thermal conductivity at low volume fractions of spherical shape nanoparticles can be defined by the Maxwell-Garnett model [35] which has gained wide acceptance

$$\frac{k_{nf}}{k_f} = \frac{k_p + 2k_f + 2\phi(k_p - k_f)}{k_p + 2k_f - \phi(k_p - k_f)}$$
(10)

where k is the thermal conductivity and ϕ denotes the nanoparticles volume concentration. Also, the subscripts nf, f, p are the nanofluid, base fluid, and particle, respectively.

The famous Brinkman relation [36] is used to find effective viscosity for a nanofluid medium containing a dilute suspension of sphere-shaped nanoparticles.

$$\mu_{nf} = \frac{\mu_f}{(1-\phi)^{2.5}} \tag{11}$$

The effective density, heat capacitance and thermal expansion coefficient, for an equilibrium condition, are considered by the following relations [37]

$$\rho_{nf} = (1 - \phi)\rho_f + \phi\rho_p \tag{12}$$

$$\left(\rho C_p\right)_{nf} = (1 - \phi)\left(\rho C_p\right)_f + \phi\left(\rho C_p\right)_p \tag{13}$$

$$(\rho \beta_t)_{pf} = (1 - \phi)(\rho \beta_t)_f + \phi(\rho \beta_t)_p \tag{14}$$

Finally, the nanofluid thermal diffusivity can be represented as [38]

$$\alpha_{nf} = \frac{k_{nf}}{\left(\rho C_p\right)_{nf}} \tag{15}$$

3.3. LBM for natural convection

The unknown macroscopic processes including change of temperature field, phase change, and fluid flow are determined using a mesoscopic solution approach namely the Lattice Boltzmann method. This approach utilizes particle distribution functions that indicate particle direction, position and time [39]. LBM simulates the phenomena by capturing an ensemble of particles and considering their collision and streaming [40,41].

Two distributions of function, f and g, are applied to fluid flow and temperature equations of a medium, respectively. In this way, macroscopic parameters distribution, i.e. velocity, pressure and temperature are determined. For this purpose, the widely used D2Q9 model is chosen in the solution procedure, as shown in Fig. 2. In this model, 2 refers to the dimension of the problems and 9 refers to the number of streaming directions

Bhatnagar et al. [42] approximated the collision term with a usable model. Using this approximation, fluid flow and temperature in LBM scheme are given as [43]

$$f_{i}\left(\overrightarrow{r}+\overrightarrow{e}_{i}\Delta t,t+\Delta t\right)=f_{i}(\overrightarrow{r},t)-\frac{\Delta t}{\tau_{v}}\left[f_{i}(\overrightarrow{r},t)-f_{i}^{(eq)}(\overrightarrow{r},t)\right]+\dot{J}_{i} \tag{16}$$

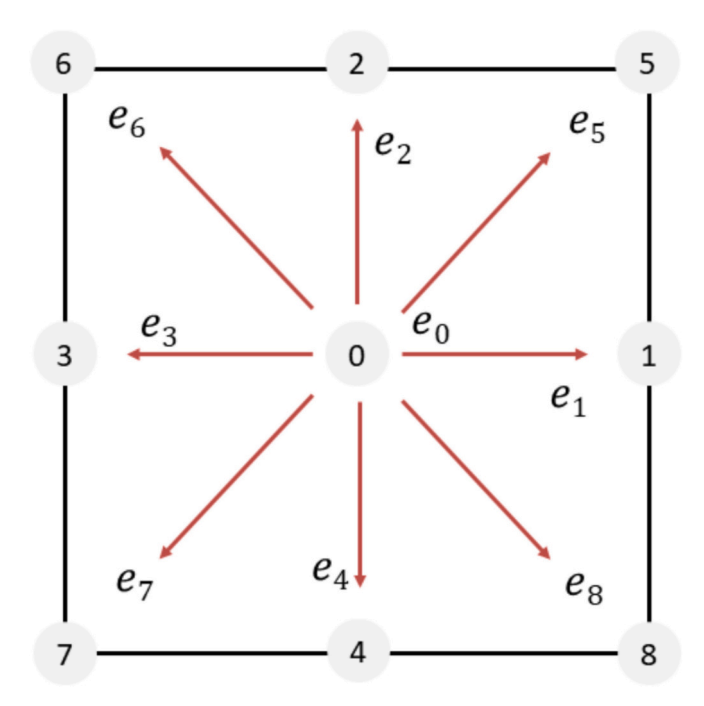


Fig. 2. Directions of D2Q9 lattice.

$$g_{i}\left(\overrightarrow{r}+\overrightarrow{e}_{i}\Delta t,t+\Delta t\right)=g_{i}(\overrightarrow{r},t)-\frac{\Delta t}{\tau_{t}}\left[g_{i}(\overrightarrow{r},t)-g_{i}^{(eq)}(\overrightarrow{r},t)\right]\\ -\left(\frac{\Delta t}{\rho C_{p}}\right)w_{i}\nabla\cdot\overrightarrow{q}_{R} \tag{17}$$

where τ_v and τ_t are the relaxation time for the flow and temperature distribution, respectively. The discrete particle velocity denoted \overrightarrow{e}_i in direction i, \overrightarrow{r} indicates the position vector, and the external force term is defined by \dot{J}_i . Also, the impact of volumetric radiation is illustrated as an extra term in the energy equation. In D2Q9 model, the discrete velocities \overrightarrow{e}_i and the weighting factors w_i are represented as follows [40]

$$\overrightarrow{e}_{i} = \begin{cases} (0,0) \\ \left(\frac{\cos(i-1)\pi}{2}, \frac{\sin(i-1)\pi}{2}\right)C & i = 0 \\ 1 \leq i \leq 4 \\ \sqrt{2}\left(\cos\frac{(2i-1)\pi}{4}, \sin\frac{(2i-1)\pi}{4}\right)C \end{cases}$$
 (18)

$$w_0 = \frac{4}{9}, w_{1-4} = \frac{1}{9}, w_{5-9} = \frac{1}{36} \left(\sum_{i=0}^{9} w_i = 1 \right)$$
 (19)

where $C = \Delta x/\Delta t$ is lattice speed and its value set to unity in this approach. The relaxation times are derived from the LB model using the Chapman-Enskog analysis and the kinetic viscosity ν and the thermal diffusivity α by follows [40]:

$$\tau_{\nu} = \frac{\nu}{G^{2} \Delta t} + \frac{1}{2} \tag{20}$$

$$\tau_t = \frac{\alpha}{C_s^2 \Delta t} + \frac{1}{2} \tag{21}$$

where $C_s = C/\sqrt{3}$ is the local lattice sound speed. $f_i^{(eq)}$ and $g_i^{(eq)}$ indicate the functions of local equilibrium distribution to satisfy macroscopic expressions. These functions are generally given as [44]

$$f_i^{(eq)} = w_i \rho \left[1 + \frac{3\left(\overrightarrow{e}_i \cdot \overrightarrow{u}\right)}{C^2} + \frac{9\left(\overrightarrow{e}_i \cdot \overrightarrow{u}\right)^2}{2C^4} - \frac{3\overrightarrow{u}^2}{2C^2} \right] \quad 0 \le i \le 8$$
 (22)

$$g_i^{(eq)} = w_i \rho RT \left[1 + \frac{3\left(\overrightarrow{e}_i \cdot \overrightarrow{u}\right)}{C^2} + \frac{9\left(\overrightarrow{e}_i \cdot \overrightarrow{u}\right)^2}{2C^4} - \frac{3\overrightarrow{u}^2}{2C^2} \right] \quad 0 \le i \le 8$$
 (22)

where ρ and T are density and temperature to be calculated, and \overrightarrow{u} is macroscopic velocity. Utilizing the Boussinesq approximation, the force term j in the flow equation under Boussinesq approximation is calculated as follows [44].

$$\dot{J}_i = 3w_i \beta_t g_v \Delta T \rho(r, t) e_{iv} \tag{23}$$

where β_t is the coefficient of thermal expansion. For buoyancy force, the gravitational acceleration g_y is considered in the vertical direction.

The two dimensionless numbers, Rayleigh number (*Ra*) and Prandtl number (*Pr*), are critical in analyzing the natural convection process and are expressed as [43],

$$Ra = \frac{\beta_t g_y (T_H - T_C) H^3}{\nu \alpha} \tag{24}$$

$$Pr = \frac{\nu}{\alpha} \tag{25}$$

Finally, macroscopic velocity and scalar quantities are obtained using following equations [43]:

$$\rho = \sum_{i} f_{i}, \overrightarrow{u} = \frac{1}{\rho} \sum_{i} \overrightarrow{e}_{i} f_{i}, T = \frac{1}{R\rho} \sum_{i} g_{i}$$
(26)

It should be noted that Mach number $Ma=|\overrightarrow{u}|\times\sqrt{3}/C$ is the parameter that determines the type of flow regime. For the assumption of incompressible flow to be true, the value of the Mach number must be <0.3 [45]. In the current research, its value is considered equal to 0.1 to achieve incompressible flow.

3.4. LBM for volumetric radiation

Volumetric radiation effects appear in the heat equation as the source term. In this term, there is a radiation flux divergence, $\nabla \cdot \overrightarrow{q_R}$ whose value is determined by solving the radiation transfer equation. This is defined as follows using the incident radiation G [31]:

$$\nabla \cdot \overrightarrow{q_R} = \kappa_a \left(4\pi \frac{\sigma T^4}{\pi} - G \right) = \beta (1 - \omega) (4\pi I_b - G) \tag{27}$$

$$G = \int_{\delta=0}^{2\pi} \int_{\gamma=0}^{\pi} I(\gamma, \delta) \sin\gamma d\gamma d\delta$$
 (28)

where $\omega = \sigma_s/\beta$, γ $(0 \le \gamma \le \pi)$ and δ $(0 \le \delta \le 2\pi)$ denote the scattering albedo, the polar angle and the azimuthal angle.

$$G = \int_{\delta=0}^{2\pi} \int_{\gamma=0}^{\pi} I(\gamma, \delta) \sin\gamma d\gamma d\delta \tag{29}$$

To obtain the radiation intensity in a participating medium, the Lattice Boltzmann method scheme is used, which are briefly reviewed. This method provided by Mishra and Asinari etc. [16,18] has many advantages compared to the numerical methods. The radiative transfer equation (RTE) can be calculated in any direction \overrightarrow{s} by the following equations [31]

$$\overrightarrow{s} \cdot \nabla I = -\beta I + \kappa_a I_b + \frac{\sigma_s}{4\pi} \int_{4\pi} I P(\Omega, \Omega') d\Omega'$$
(30)

$$\widehat{s} = (\sin\gamma\cos\delta)\widehat{i} + (\sin\gamma\sin\delta)\widehat{j} + \cos\gamma\widehat{k}$$
(31)

where $I_b = \sigma T^4/\pi$ is intensity of the black body and $\sigma = 5.67 \times 10^{-8} \text{ W/m}^2\text{K}^4$ signifies the Stephan-Boltzmann constant. Moreover, P indicates the scattering phase function. Using the assumption of Asinari et al. such as local equilibrium and time-dependent condition, the radiation equation is modified as follows [16]:

$$\frac{1}{c}\frac{\partial I_i}{\partial t} + \overrightarrow{s} \cdot \nabla I_i = \beta \left(\frac{G}{4\pi} - I_i\right) \tag{32}$$

where c and I_i are the light speed and radiation intensity travelling for direction i. Accordingly, the LBM formulation for radiation intensity is given as [16]

$$I_{i}(\overrightarrow{r}+e_{i}\Delta t,t+\Delta t)-I_{i}(\overrightarrow{r},t)=-\frac{\Delta t}{\tau_{i}}\left[I_{i}(\overrightarrow{r},t)-I_{i}^{(eq)}(\overrightarrow{r},t)\right] \tag{33}$$

where the relaxation time for the collision of intensities is $\tau_i = 1/e_i\beta$. The equilibrium distribution functions I_i^{eq} and corresponding weight factors w_{gi} are determined by [16]

$$I_i^{(eq)} = \sum_{i=1}^{M} I_i w_{gi}$$
 (34)

$$w_{gi} = \frac{1}{4\pi} \int_0^{\pi} \sin\gamma d\gamma \int_{\delta_i - \frac{\Delta \delta_i}{2}}^{\delta_i + \frac{\Delta \delta_i}{2}} d\delta = \frac{\Delta \delta_i}{2\pi}$$
 (35)

In a two-dimensional domain, the D2Q8 model is sufficient for the radiation equation due to no rest population of distribution function. So, 2π angular space is considered for each direction as shown in Fig. 3. The velocity of these directions are represented as follows [16]

$$e_{1,3} = (\pm 1, 0) \cdot \frac{\Delta x}{\Delta t}, e_{2,4} = (0, \pm 1) \cdot \frac{\Delta x}{\Delta t}, e_{5,6,7,8} = (\pm 1, \pm 1) \cdot \frac{\Delta x}{\Delta t}$$
 (36)

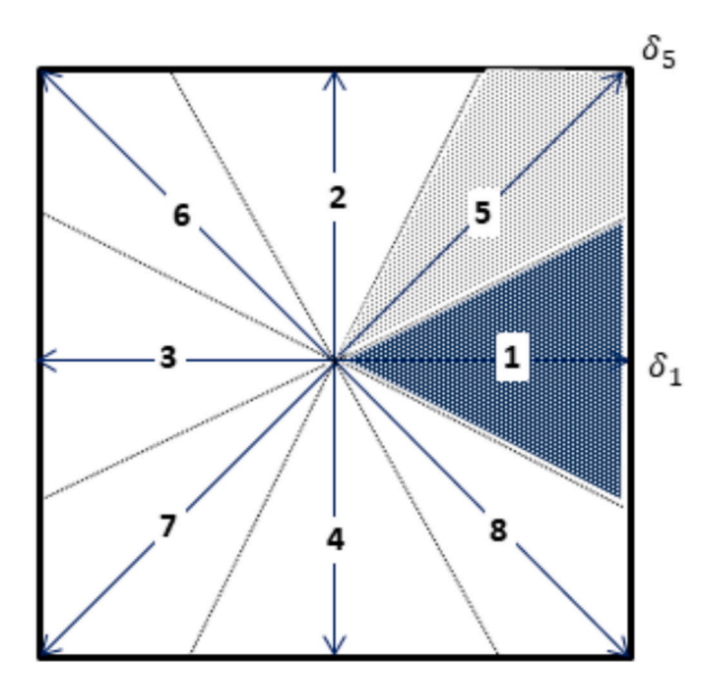


Fig. 3. 1-8 directions of the D2Q8 lattice for radiation equation.

3.5. LBM for conductive PCM

The LBM approach is also used to solve the energy equation for the PCM block in order to simulate the phase change. The existing methods for modelling phase change in this approach are classified into two groups: 1. The phase field methods based on the theory stated by Ginzburg-Landau [46,47]; 2. The enthalpy-driven methods [48,49]. In the current research, the enthalpy-driven technique provided by Jiaung et al. [48] is used to find the temperature distribution and fraction of the melting amount over time.

The phase change term appears in the energy equation, which behaves as a heat source or sink. It is included in the collision step of solving the Lattice Boltzmann equation. It is worth mentioning that in the PCM block, the assumptions of zero velocities, negligible radiation power, and properties different from nanofluids are considered. Therefore, the energy equation in the LBM form for the PCM block is as follows [50]:

$$g_i^{n,k+1}(x+e_i) = g_i(x) - \frac{1}{\tau_h} \left(g_i(x) - g_i^{eq}(x) \right) - w_i \frac{L_f}{c_p} \left(f_l^{n,k}(x) - f_l^{n-1}(x) \right)$$
(37)

where c_P , Lf, and f_l are specific heat capacity, latent heat of phase change, and liquid fraction, respectively. Therefore, in this area, the macroscopic temperature can be calculated from the following equation [48]

$$T^{n,k} = \sum_{i=0}^{4} g_i^{n,k} \tag{38}$$

where $T^{n,k} \equiv T^k(t=n)$. The local enthalpy can be computed as below [48]:

$$En^{n,k} = c_p T^{n,k} + L_f f_I^{n,k-1}$$
(39)

The liquid fraction at each time step is determined locally using enthalpy as follows [48]

$$f_{l}^{n,k} = \begin{cases} 0 & En^{n,k} < En_{s} = cT_{m} \\ \frac{En^{n,k} - En_{s}}{En_{f} - En_{s}} & En_{s} \leq En^{n,k} \leq En_{s} + L_{f} \\ 1 & En^{n,k} > En_{s} + L_{f} \end{cases}$$
(40)

The temperature and liquid fraction are calculated by converging to a specified value in each iterating. The time step n+1 is determined through a similar process. In the phase change problem, two dimensionless numbers, Stefan number St and Fourier number Fo, are crucial. These numbers are defined as follows [51]:

$$St = \frac{c_p \left(T_C - T_m\right)}{L_f} \tag{41}$$

$$Fo = \frac{\alpha t}{t^2} \tag{42}$$

The Fourier number is a dimensionless time indicator that is used to better analyze the phase change behavior as a transient phenomenon. Therefore, the results under different conditions are reported in the same Fourier number for better comparison.

3.6. LBM treatment for conjugate heat transfer

As mentioned, temperature distribution and phase change analysis in the PCM block are part of the results considered in this research. Due to the different thermophysical properties of the material inside the block and the nanofluid, assorted equilibrium distribution functions and relaxation time are employed for each phase. In order to apply the heat transfer balance in the block boundaries, a row of interfacial nodes is considered from the study of Seddiq et al. [52].

Consequently, the distribution function related to the temperature equation can be directly calculated. To calculate the unknown distribution function at the interface, it is assumed that the gradient of the distribution function in the direction perpendicular to the boundary is related to the ratio of solid to liquid conductivity coefficient, i.e.

$$R_k \left(\frac{\partial g_k}{\partial x.y} \right)_{PCM} = \left(\frac{\partial g_k}{\partial x.y} \right)_{nf}$$
. R_k is the ratio of PCM to nanofluid thermal

conductivity. In this way, the energy transferred from the fluid to the block is modelled at each lattice node, and the values are updated during the time marching step. Therefore, the distribution function at the interface is calculated as follows [25]

$$g_k(x_i, y_i) = \frac{g_k(x_f, y_f) + R_k g_k(x_s, y_s)}{1 + R_k}$$
(43)

where i, f, b refer to interface, fluid, and block nodes, respectively. According to above equation, the temperature of interface can be computed easily as follow

$$\theta(x_i, y_i) = \frac{\sum_k g_k(x_f, y_f) + R_k \sum_k g_k(x_s, y_s)}{1 + R_k}$$
(44)

It is worth mentioning that with the temperature update for each time step, the radiation intensity from the boundaries of the PCM block is also revised.

3.7. LBM for boundary conditions

Implementing appropriate boundary conditions for combined heat transfer problems is one of the most important tasks. In the flow equation, the distribution functions are known on the boundaries, while their values are unknown inside the fluid domain. Therefore, the distribution functions inside the solution domain must be defined on the boundaries. For the walls of the enclosure and the block, the bounce back boundary condition is used. This way, the particles return to the solution domain in the opposite direction, and the zero velocity condition is satisfied. So, the post-collision distribution function can be known as follows for each node at wall boundaries [43]

$$f_k = f_{\bar{k}} \tag{45}$$

where the \tilde{k} shows the opposite direction of k. In the energy equation, the boundary conditions for the walls with a constant temperature are presented as follows in order to define the unknown distribution functions [48]

$$g_{kt} = T_w - \sum_{k \neq kr} g_k \tag{46}$$

where the kt denotes the unknown distribution function. In insulated walls, using the definition of heat flux at the boundaries, unknown distribution functions and temperature are determined according to references [32, 53].

The boundary conditions to achieve the unknown radiation distribution functions are determined by defining the radiative intensity from the gray and diffusion boundaries. Therefore, the radiative intensity equation is expressed as follows [32]

$$I_{w} = \frac{\varepsilon \sigma T_{w}^{4}}{\pi} + \left(\frac{1-\varepsilon}{\pi}\right) \times \int_{\overrightarrow{n} \cdot \overrightarrow{\Omega} < 0} \left| \overrightarrow{n} \cdot \overrightarrow{\Omega} \right| I\left(r, \overrightarrow{\Omega'}\right) d\Omega'$$
(47)

where ε and \overrightarrow{n} are emissivity and the unit vector of boundaries toward fluid domain. In this equation, I_w is the radiation intensity leaving the boundary surface and $I\left(r,\overrightarrow{\Omega'}\right)$ is the radiation intensity in Ω' direction arriving at that surface. If the walls are considered black surfaces ($\varepsilon=1$), the above equation can be reduced as $I_w=\sigma T^4/\pi$. So, the radiation temperature is retrieved from the temperature field boundary condition.

4. Numerical solution procedure

In the current simulation, the full LBM method determines the flow, temperature, and radiation intensity distribution in the solution domain by benefiting from three distribution functions: f, g, and I. To solve the equations in this method, a single relaxation time model was used for the collision term. The time step and the grid size in the LBM approach are chosen to be 1, which are in lattice units. The target problem is the natural convection and volumetric radiation of Al_2O_3 -water nanofluid in a two-dimensional enclosure containing a block of phase change material (paraffin). The procedure of the solution method in the LB scheme is summarized as follows:

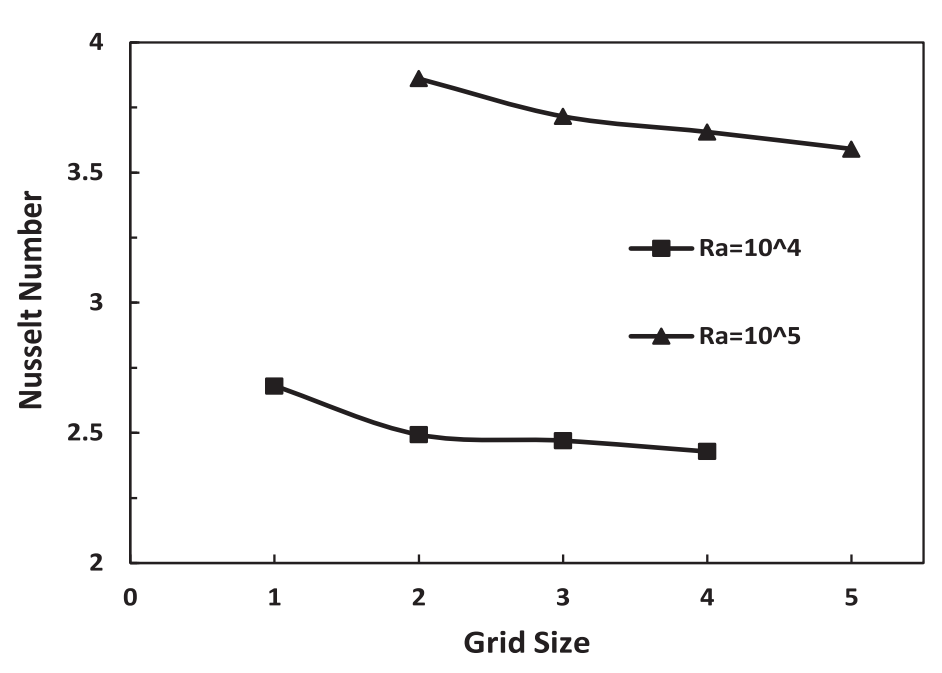


Fig. 4. Grid independency of Nusselt number at different Ra.

Table 4Comparison of average Nusselt number.

φ (%)	Ra	Ref. [54]	Present	Relative error %
1 2	10 ⁵ 10 ⁵	4.86 5.00	4.99 5.16	2.68 3.20
3	10 ⁵	5.14	5.29	2.91

 Table 5

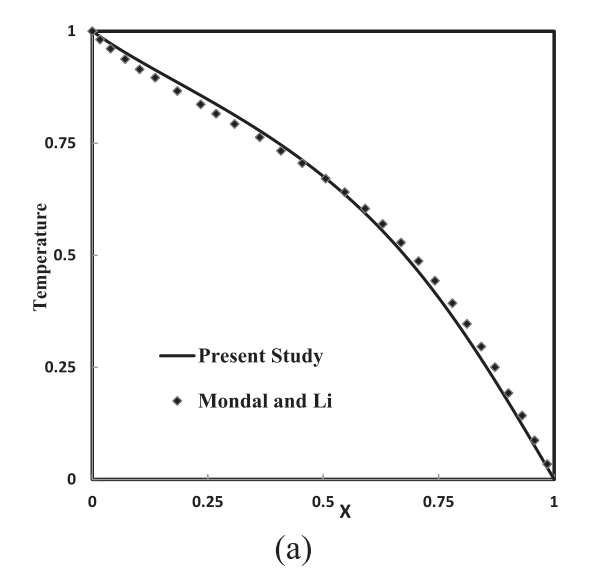
 Comparison of average Nusselt number with experimental results.

Ra	Ref. [55]	Present	Relative error %
1.02×10^5	10.49	10.19	2.9
1.68×10^{5}	11.89	11.68	1.76
2.11×10^{5}	12.71	12.53	1.43

- Provide constant parameters and compute the relaxation times of governing equations.
- Set boundary conditions and apply the required initial values.
- Compute the local functions of equilibrium distribution.
- Calculate the radiative intensity distributions I_i and ∇· qR needed in the energy equation.
- Perform collision and streaming steps to determine the f_i and g_i of flow and energy, respectively.
- In the area related to the PCM block, the collision term of the energy equation is determined according to the temperature value (material phase).
- Update the total enthalpy and the liquid fraction in the block domain by repeating the solution in a time step.
- Determine the macroscopic quantities in the solution domain.
- Update the distribution functions of velocity, temperature and intensity for satisfying the boundary conditions.
- Go to the step of calculating the equilibrium distribution functions.
- Repeat the iterative steps until convergence criteria are met for the macroscopic variables. The maximum relative error between two iterations is considered 10^{-6} at each time step. The phase change process is a transient phenomenon that requires an appropriate time step to achieve correct results in an optimal runtime. In this study, a dimensionless time step of 1.5×10^{-6} was taken after examining the sensitivity of time discretization.

5. Mesh independency and method verification

To investigate the effect of mesh size on the accuracy of the simu-



lation results, a conducting PCM block size of 25 % was placed in the center of the physical domain filled with $\rm Al_2O_3$ -water nanofluid, Fig. 1 (b). The average Nusselt number $\it Nu$ of natural convection for the hot wall, at a nanofluid concentration of 0.3 %, was examined for two different Rayleigh numbers of 10^4 and 10^5 . Fig. 4 shows an optimal grid size for each Rayleigh number to achieve valid results. In this way, 128 \times 128 and 256 \times 256 grids are suggested for Rayleigh numbers of 10^4 and 10^5 , respectively.

At first, a comparison of the Al_2O_3 nanofluid natural convection with the numerical results of Lai and Yang [54] is presented. For this purpose, the Nusselt number on the enclosure wall was compared for three different concentrations of nanofluid at the Rayleigh number of 10^5 , as shown in Table 4. From this table, the maximum relative error is 3.2 %, which indicates the accuracy of pure natural convection results for a nanofluid.

To validate the current code, it is necessary to compare the results with previously published experimental works. These validations were carried out during the simulation of natural convective heat transfer in a square cavity in the presence of a hot block with the experimental results of Paroncini and Corvaro [55]. The examination of the average Nusselt number on the lateral surfaces displays close conformity with the findings of Paroncini and Corvaro [55], as shown in Table 5.

To validate the accuracy of the LBM presented in this paper for combined volumetric radiation and natural convection, the dimensionless temperature at the midplane of a 2D enclosure (along the Y = 0.5) was compared with the data of Mondal and Li [28]. The results for validation cases were plotted in Fig. 5. These comparisons are provided for two different Rayleigh numbers of $Ra=10^3$ and 10^4 at Prandtl number Pr=0.71, extinction coefficient $\beta=1$ and albedo scattering $\omega=0.0$.

Fig. 5 reveals a very good agreement between the results so that the maximum relative error was 7.6 %. The primary source of deviation could be that the numerical solution method in this study is full LBM, while in the reference paper, the finite volume method was used for the RTE. The approximations used in the mathematical modelling of both methods as well as the convergence criterion could cause differences in the results. Hence, demonstrating sufficient accuracy of the numerical model presented in this study for simulating coupled natural convection with volumetric radiation.

Finally, in order to investigate the presented method for solving the phase change of material in the block, the problem of solidification with dominant conduction in a semi-infinite corner is considered. At the starting moment, the solution domain is in the liquid phase and the

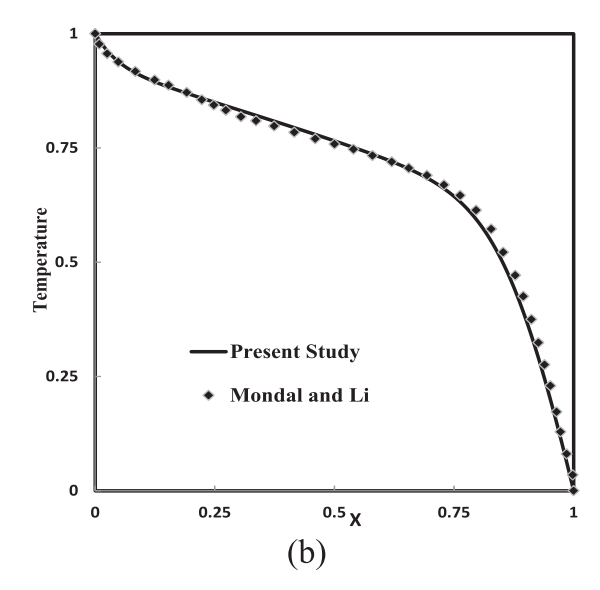
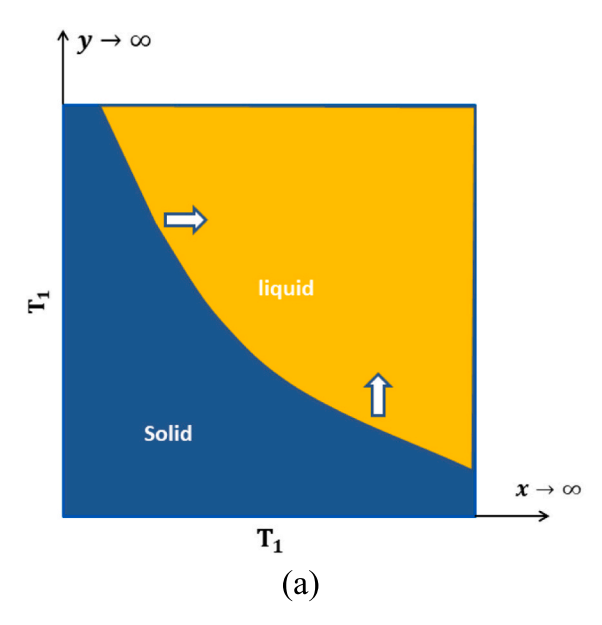


Fig. 5. Validation of dimensionless temperature distribution at Y=0.5 mid-plane of cavity for $\beta=1$ and $\omega=0.0$ and for (a) $R\alpha=10^3$ and (b) $R\alpha=10^4$.



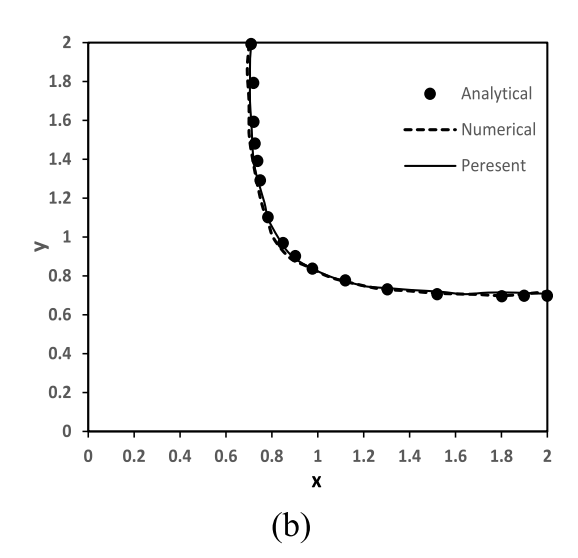


Fig. 6. (a) The coordinate system of a semi-infinite corner for solidification problem. (b) Comparison of temperature from the analytical solution with LBM results.

initial temperature is set to 0.3. Then the temperature decreases to -1 at the boundaries of x=0 and y=0 (Fig. 6(a)). The temperature of the solidification point is considered to be 0, so the phase change starts from these boundaries.

To solve the problem, Stephen number, St, has been assumed to be 4. The results of analytical and numerical solution of this problem from previous litterateurs [56,57] are compared with the results of the LBM approach presented in this article for the Fourier number of 0.25 in Fig. 6(b). It was observed that the present results are in good agreement with the results of the numerical and analytical solutions, so the presented method is valid for simulating the phase change process.

6. Results and discussion

It should be remembered that the current study is an investigation of the combined problem of volumetric radiation considering the optical properties of nanoparticles with natural convection in the presence of PCM block, which is a model of the heat storage and exchange process in energy systems. Computations were performed on a uniform grid through the lattice Boltzmann method. Effects of the presence of volumetric radiation, Rayleigh number, PCM block size, plank number, and nanofluid concentration on the results such as phase change propagation, flow and temperature distribution, and liquid fraction are discussed.

6.1. Radiation effects

Fig. 7 shows the liquid fraction in the PCM block for both with and without considering radiation at Rayleigh 10^4 for four different Fourier numbers. Also, nanofluid concentration, Planck number, Stefan number, and block size are 0.3 %, 0.01, 0.5 and 50 %, respectively. Fig. 7(a), which is related to pure natural convection, indicates that the phase change within the PCM block starts at the left and upper boundary.

The melting progresses over time so that at the Fourier number of 0.38 the upper of the diagonal of the PCM block is completely changed to liquid. The reason for this observation can be stated that for the Rayleigh number of 10^4 , the effects of conduction and natural convection are both significant, so the temperature gradient extends from the side of the hot wall (left boundary) and the upper horizontal wall. As a result, heat is transferred from these areas to the PCM block, which causes a phase change process.

Fig. 7(b) illustrates completely different liquid fraction results for the combination of natural convection and volumetric radiation. In this condition, the phase change in the PCM block begins to progress from the top, left and bottom walls, which indicates that the boundaries of the input heat to the block are different. In the presence of volumetric radiation, heat radiation is transferred from the hot wall to the PCM block through the nanofluid, so the PCM block receives more heat even from the lower boundary.

The results of the liquid fraction distribution in the PCM block can be better understood by observing the transient temperature contours that will be presented in the following. It was also found that at the same Fourier number for considering the radiation, the liquid fraction increases intensely compared to pure natural convection. For example, at the Fourier number of 0.38, the liquid fraction is 81 % for the combined heat transfer, while without considering the radiation 48 % of PCM is melted. This result proves that if volumetric radiation is considered, more amount of the PCM block changes phase in equal time, consequently, more capacity is used for energy storage.

The physical reason for this result can be stated that under the pure natural convection, thermal energy is transferred from the hot boundary layers to the PCM via natural convection heat transfer. However, when volumetric radiation is introduced, radiative thermal energy can also be contributed within the fluid bulk based on the optical properties of the nanofluid.

Fig. 8 shows the temperature distribution in the solution domain at Rayleigh number of 10^4 for the case of pure natural convection and in combination with volumetric radiation. From Fig. 8(a), without radiation, at the smallest Fourier number (0.028), the temperature gradient extends from the hot boundary and the upper regions, so that the temperature of the nanofluid increases near the upper adiabatic wall and the left wall. For larger Fourier numbers, the increase in temperature is observed in the entire solution domain and the temperature gradient is created in the nanofluid and the PCM block.

This temperature distribution is due to the buoyancy effect and heat transfer from the hot wall. Therefore, the fluid near the left boundary and the upper horizontal boundary of the block has a higher temperature. This is because the heat transfer from the hot wall to the nanofluid reduces its density, so the hot fluid moves upwards due to buoyancy effects. As a result, more heat is transferred from these areas to the PCM block, beginning the melting process.

In the presence of volumetric radiation, the isotherms are distributed

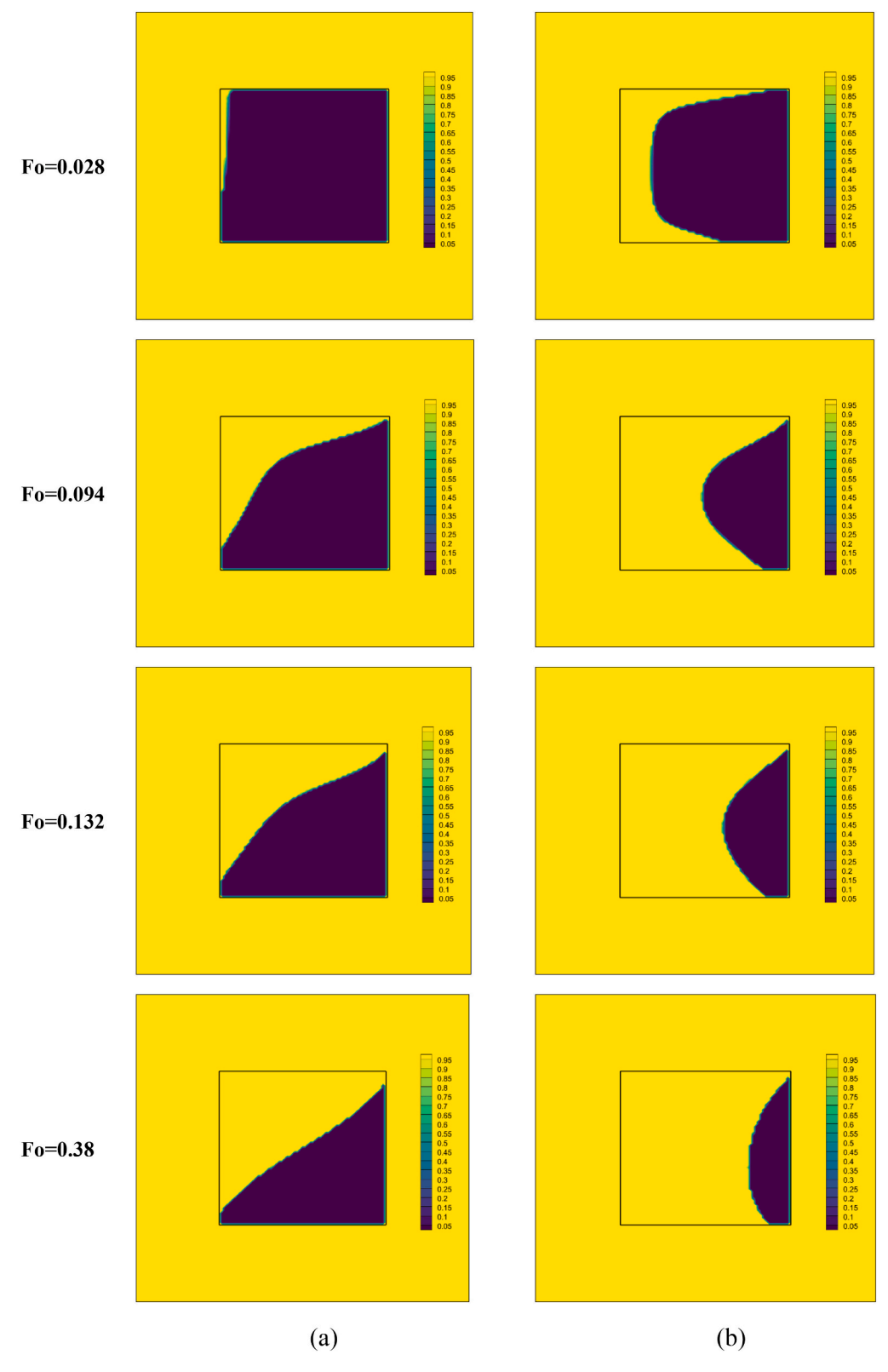


Fig. 7. Liquid fraction for $Ra=10^4$ at $\phi=0.3\%, pl=0.01$ and block size =50%. (a) Pure natural convection (b) Radiation and natural convection.

completely differently. From Fig. 8(b), an increase in temperature is observed near the lower boundary, and the enclosure temperature also increases significantly for all Fourier numbers compared to pure natural convection. Therefore, heat is transferred to the PCM block through the upper, lower and left boundaries. Moreover, the heat transferred became

higher for the radiation presence at the same Fourier number. The isotherms of the nanofluid are almost vertical and the temperature gradient is lower in the areas near the hot wall due to heat radiation.

Therefore, the increase in heat transfer due to the influence of the radiation contribution is clearly observed in the temperature

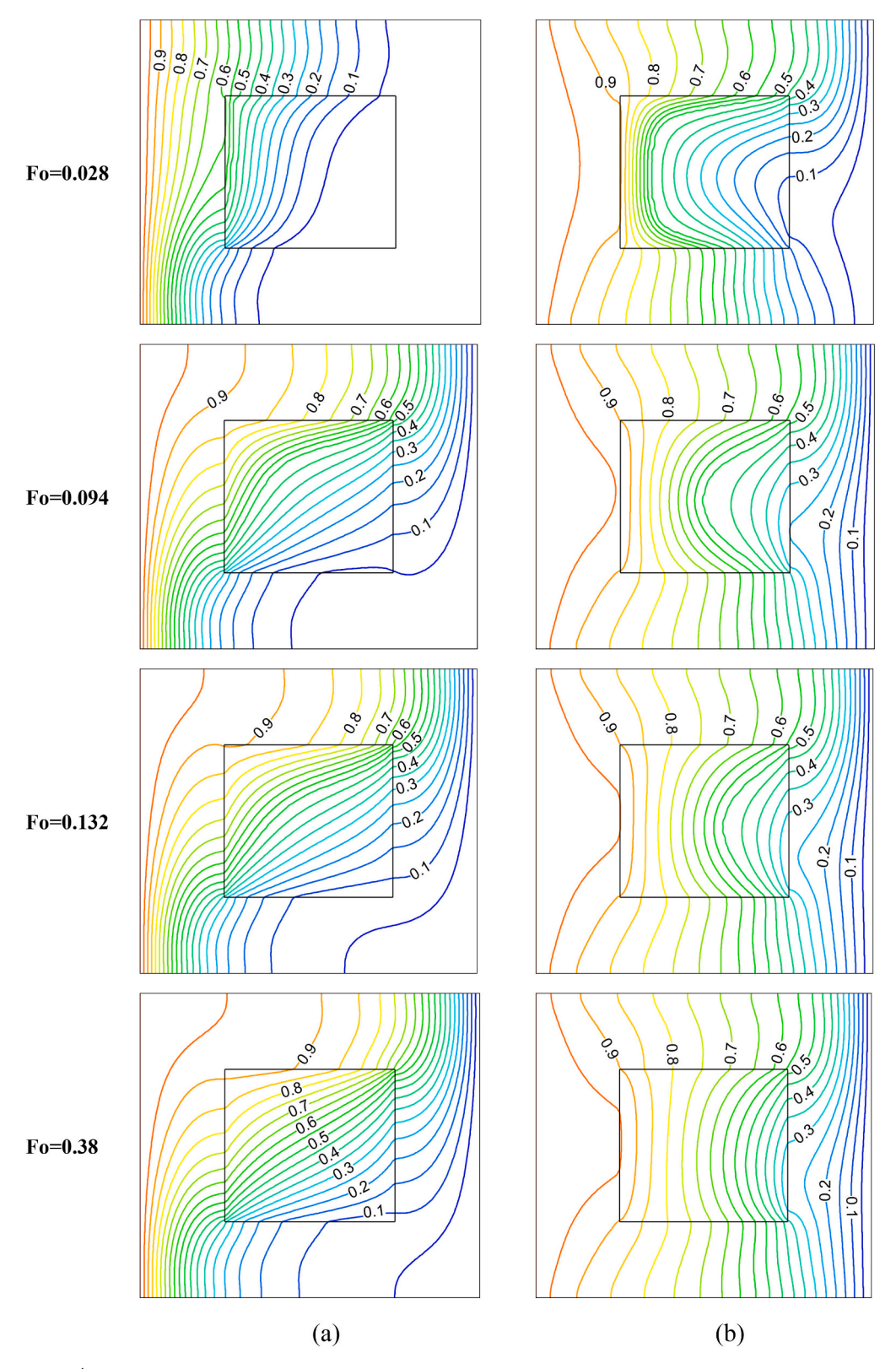


Fig. 8. Isotherm for $Ra=10^4$ at $\phi=0.3\%, pl=0.01$ and block size =50%. (a) Pure natural convection (b) Radiation and natural convection.

distribution. This result can also be justified using the source term related to the radiative heat flux in the energy equation. The presence of a radiative flux gradient in this equation improves heat transfer, increasing the temperature of the medium. This leads to temperature uniformity in the upper and lower regions of the enclosure, unlike pure

natural convection.

Fig. 9 displays the propagation of the phase change within the PCM block in terms of time for two conditions with and without radiation at a larger Rayleigh number, 10^5 (stronger natural convection). As can be seen from this figure, for the case of pure natural convection at the

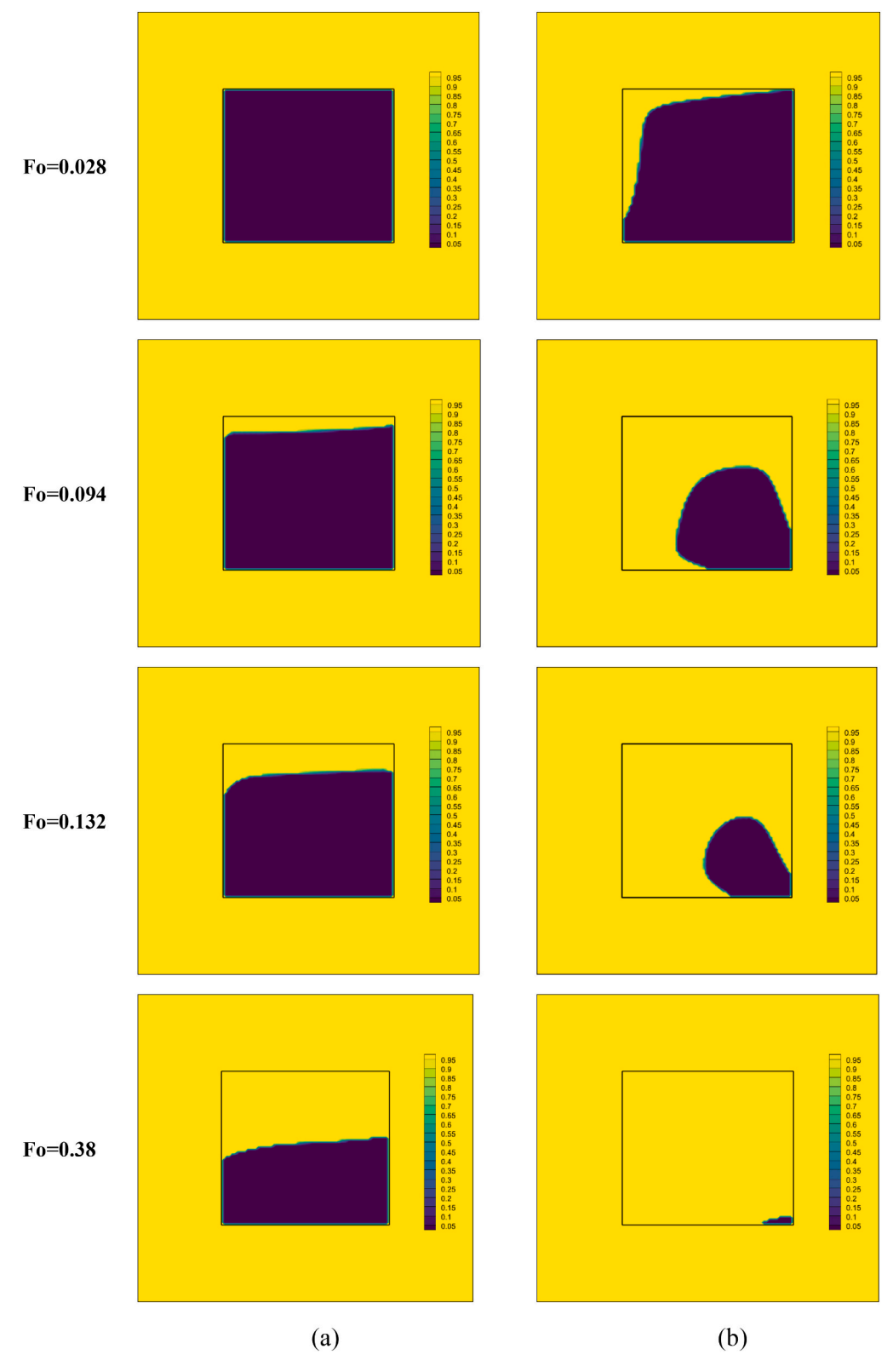


Fig. 9. Liquid fraction for $Ra=10^5$ at $\phi=0.3\%, pl=0.01$ and block size =50%. (a) Pure natural convection (b) Radiation and natural convection.

Fourier number of 0.028, no phase change occurred in the block. As the Fourier number increases, the phase change starts from the top of the PCM block. This result is because the nanofluid near the hot wall is heated and the natural convection process starts. Subsequently, the nanofluid flows to the upper area of the enclosure faster compare to the

previous case due to a higher buoyancy effect. Thus, the PCM block starts to heat up from the upper boundary.

The time-dependent liquid fraction for the combination of natural convection and radiation indicates a different behavior. In this case, the phase change starts from the upper and left boundaries, also, the rate of

phase change increases significantly. At the largest Fourier number (the Fourier number of 0.38), the liquid fraction in the PCM block for pure natural convection is almost equal to 47 %. While considering radiation, almost the entire PCM has turned into liquid (liquid fraction equal to 99 %).

This result is due to the combination of two modes of heat transfer simultaneously. So, the radiation from the wall causes an increase in heat transfer from the left boundary of the block, and natural convection, which is more intense at the Rayleigh number of 10^5 , also causes heat transfer from the upper boundary of the block. As a result, the propagation behavior of the phase change alters and the melting rate

increases significantly. These results can be interpreted by examining the transient temperature distribution in the conditions with and without radiation. It is worth noting that an important result that can be obtained from this simulation is that if radiation is omitted, an incomplete phase change may occur in the PCM block while receiving heat over a certain period of time; consequently, its full capacity is not used for energy storage.

Fig. 10 shows the temperature distribution for the nanoparticle concentration of 0.3 % and the Rayleigh number of 10^5 for two conditions without considering radiation and with radiation. Transient results are shown for four different Fourier numbers to determine how the

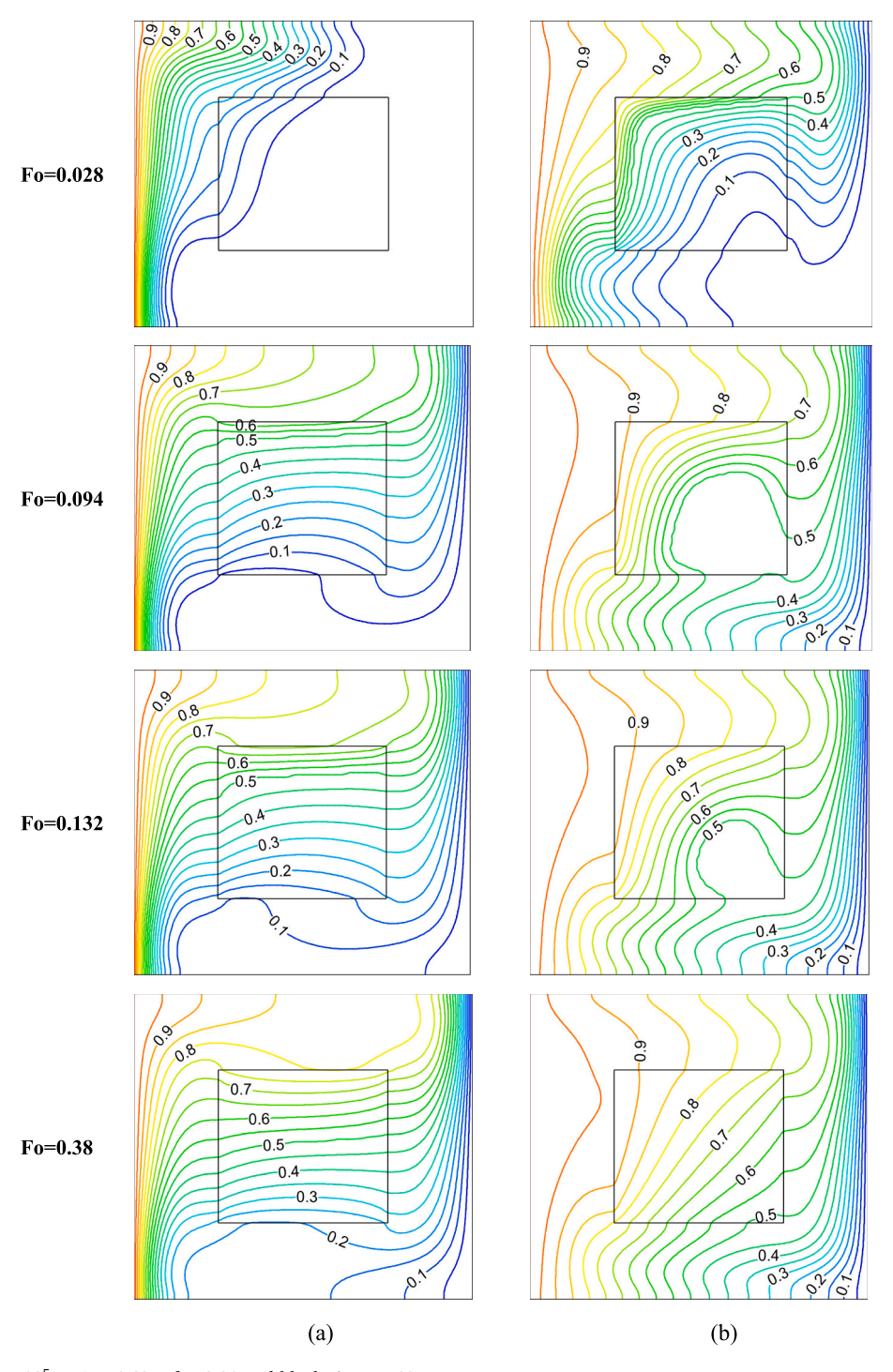


Fig. 10. Isotherm for $Ra=10^5$ at $\phi=0.3\%$, pl=0.01 and block size =50%. (a) Pure natural convection (b) Radiation and natural convection.

temperature changes in the solution domain with time. As can be seen in Fig. 10(a), regardless of the volumetric radiation, the isotherms are more compact at the bottom of the hot wall, while in the upper region of the enclosure, the isotherms are distributed due to the buoyant flow.

Over time, the temperature gradient illustrated that a high-temperature nanofluid exists at the top of the PCM block and there is a cold nanofluid at the bottom. In this way, the isotherms tend to become nearly horizontal parallel lines inside the PCM block. Hence, as mentioned before, the melting propagation starts from the upper area of the PCM block without considering radiation. In this case, natural convection and the effect of buoyancy force are dominant, so the upper area of the block changed to liquid due to contact with the higher temperature area.

Fig. 10(b) shows different results of the changes in temperature over time when volumetric radiation is taken into account. At the Fourier number of 0.028, the temperature contour indicates that the isotherms in the solution domain are more distributed compared to the without radiation results, and the temperature gradient is observed almost in the total of nanofluid and PCM block. Another main difference that can be observed is that in this case, the high-temperature nanofluid is located on the left and upper side of the PCM block. So, the isotherms inside the PCM block in the presence of radiation are not horizontal.

Over time, they change shape obliquely and almost parallel. These results can be justified by considering the radiation, the heat transfer from the hot wall will increase significantly and the temperature of the nanofluid near the radiant hot wall will increase intensively. Therefore, the combination of the effects of natural convection and volumetric radiation makes the left and upper sides of the PCM block have higher temperatures, unlike the pure convection situation, and the melting process starts from these areas. In addition, it can be seen that the temperature of the solution domain increases in the presence of radiation. So, at the Fourier number of 0.38, the temperature of the entire block for radiation presence is higher than the melting temperature.

6.2. Planck number and block size effects

The previous section showed that considering radiation can significantly affect temperature distribution, phase change behavior, and liquid fraction. This section aims to assess the effect of the Planck number $Pl = \frac{k_{nf}/H}{4\sigma T_0^3}$ (ratio of thermal conductivity to radiation) as the main parameter for the amount of radiation heat transfer effects on fluid flow and overall heat transfer. In this dimensionless number, T_0 is the reference temperature, which is described as the average of the hot and cold temperatures.

In radiative heat transfer, in addition to the temperature difference, the magnitude of the cold and hot temperatures is important. Therefore, at a constant temperature difference, when the cold and hot temperatures are higher, the reference temperature will be higher and as a result the Planck number will be smaller. Consequently, the effects of radiation are intensified in this condition. Figs. 11 and 12 show the temperature contour and streamlines, respectively, for the Rayleigh number 10^5 and Fourier number 0.38 to highlight the effect of the Planck number on temperature distribution and flow structure, and energy storage.

For all three PCM block sizes of 25, 50 and 75 %, the high temperature thermal layer is created near the hot wall at Planck number of 0.01. The isothermal lines near the cold wall are more dense. This observation can be attributed to the exchange of radiation thermal flux between the hot wall and the medium, resulting in nanofluid warming along the hot wall, and gradients near the cold wall become more intense. This result shows that the radiation effects are very significant for the Planck number of 0.01.

The isothermal lines are different from the resulting temperature distribution due to the buoyancy force in pure natural convection. The dominant effects of radiation at lower Planck numbers are due to the fact that to reduce this dimensionless number for a given nanofluid, the

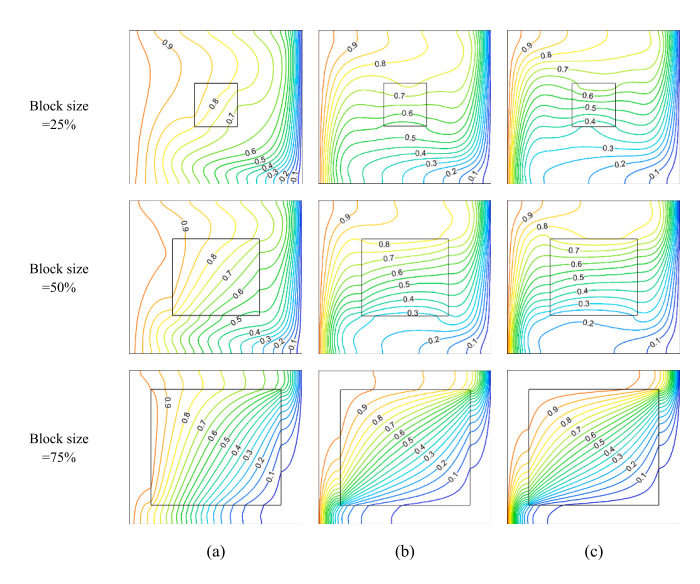


Fig. 11. Isotherms at $\phi=0.3\%$ and $Ra=10^5$ of radiation and natural convection for (a) pl=0.01, (b) pl=0.1 and (c) pl=1.

reference temperature must be increased. Increasing the reference temperature, which is the result of increasing the hot and cold temperatures, enhances the contribution of heat radiation.

With the increase in the Planck number, the isothermal lines are compressed at the bottom of the hot wall and the top of the cold wall. Moreover, the nanofluid has a higher temperature in the upper half of the solution domain and a lower temperature in the lower half. Therefore, the temperature contour is similar to the pure natural convection behavior. Accordingly, with the increase of the Pl, the effects of volumetric radiation are weaker and the buoyancy effects play a main role. It should be noted that with the increase in the size of the PCM block, the blockage effect prevents circulation and heat transfer through the nanofluid, so the temperature of the nanofluid and the PCM block is reduced especially in the lower and right regions.

Fig. 12 also shows that in all three Planck numbers, a rotating flow in the clockwise direction causes the heated fluid to rise along the left wall, collide with the upper adiabatic wall, move toward the cold wall come down and turn around again. Consequently, a single vortex around the cavity forms. This circulation in Planck 0.01 is more intense, and the symmetric flow circulation is generated around the PCM block. While increasing the Planck number, the fluid rotation is weakened and the streamlines of the ellipse are formed, which is more visible for the smaller PCM block. This is due to the attenuation of heat radiation and the reduction of heat transfer to the nanofluid. Thus, the processes of fluid flow and heat transfer are controlled by natural convection at higher Planck numbers.

In order to provide a quantitative comparison of the contribution of radiation to the total heat transfer from the hot wall into the medium, the ratio of the radiation Nusselt number to the total Nusselt number for three Planck numbers of 0.01, 0.1, and 1 at two Rayleigh numbers of 10^4 and 10^5 with a PCM block size of 25 % is shown in Fig. 13. As can be seen in this figure, the contribution of radiation to heat transfer decreases significantly with increasing Planck number, so that for both Rayleigh numbers, with the Planck number rising from 0.01 to 1, the ratio of the radiation Nusselt number to the total Nusselt number attenuates from >90 % to <1 %. These results indicate that in this problem, at Planck number 1 or larger, radiation has a negligible contribution to the total heat transfer that can be neglected. In contrast, the contribution of radiation dominates at smaller Planck numbers, which completely changes the temperature distribution.

The effects of decreasing heat transfer to PCM by increasing the Pl values can significantly reduce energy storage. To quantitatively examine this, Fig. 14 shows the liquid fraction for three Planck numbers

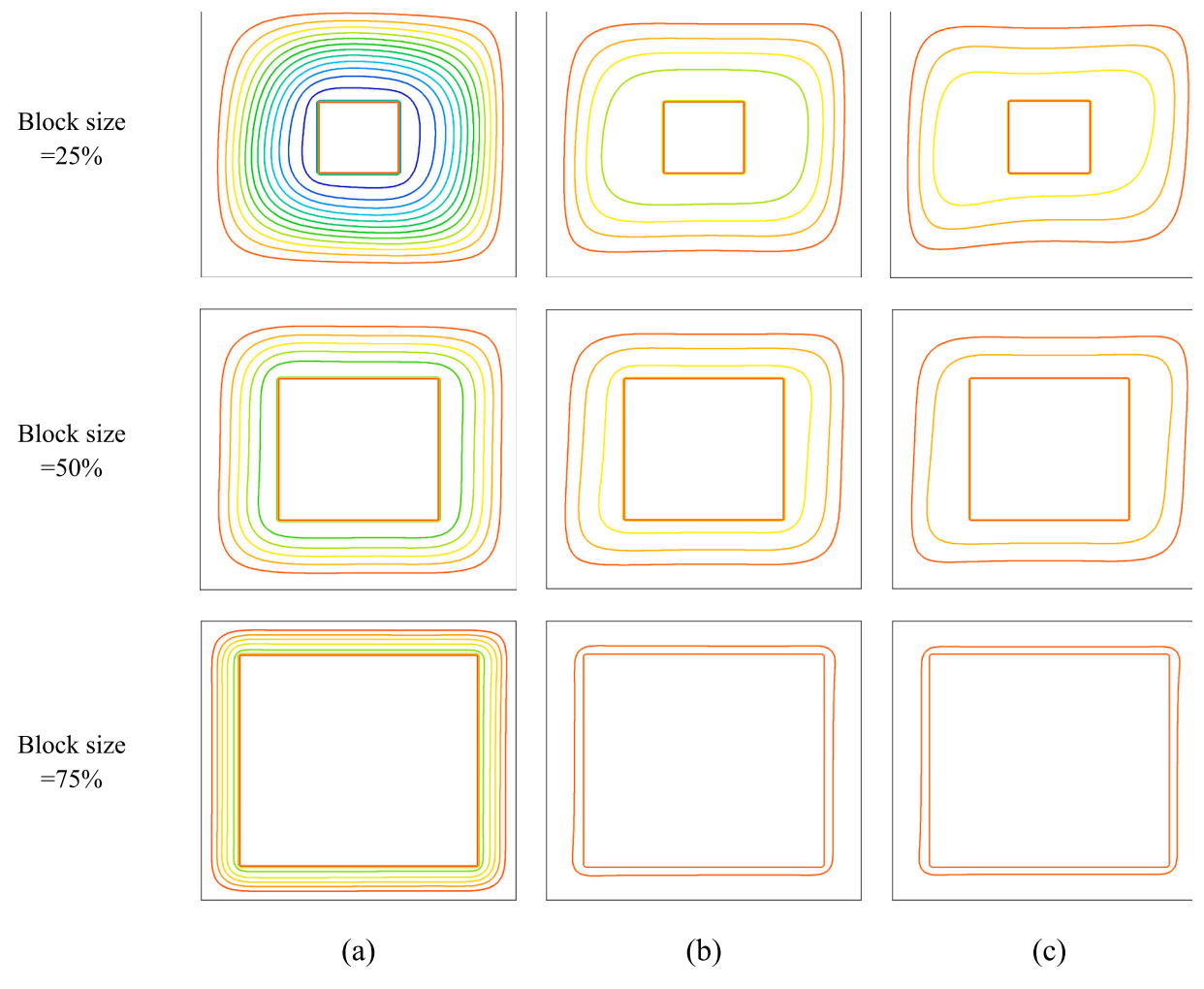


Fig. 12. Streamlines at $\phi = 0.3\%$ and $Ra = 10^5$ of radiation and natural convection for (a) pl = 0.01, (b) pl = 0.1 and (c) pl = 1.

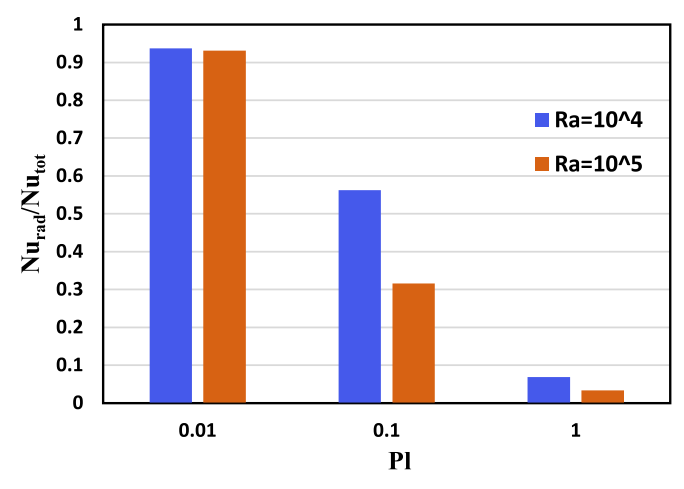


Fig. 13. Ratio of radiative Nusselt number to total Nusselt number.

of 0.01, 0.1, and 1 as a function of block size at a given time (Fourier number 0.38). As shown in this figure, the liquid fraction decreases with increasing Planck number for all three PCM block sizes. For example, in the block size of 50 % with the increase of Planck from 0.01 to 0.1 and then to 1, the value of the liquid fraction decreases from 99 % to 62 % and 49 %, respectively. So, by increasing the plank number, which subsequently reduces the effects of radiation, less phase change occurs in

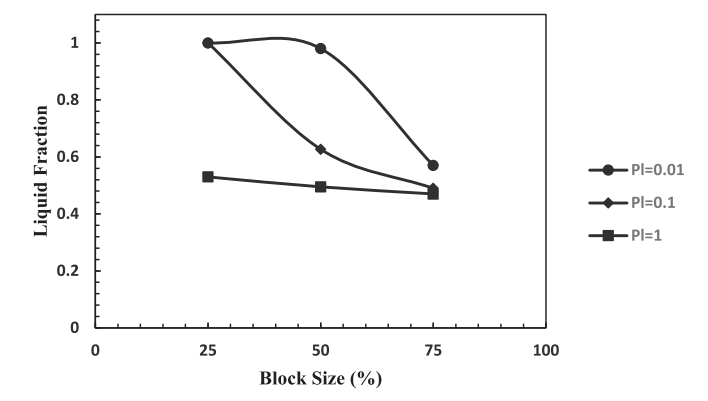
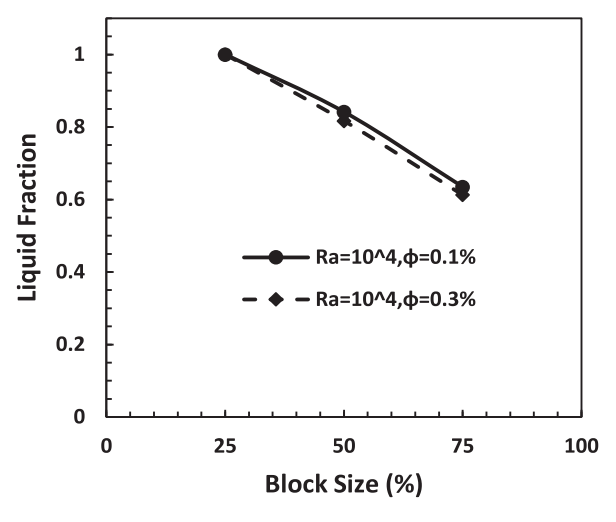


Fig. 14. Liquid fraction for different Planck number and PCM block size at $Fo=0.38, \ \phi=0.3\%$ and $R\alpha=10^5.$

a given time. This may make it impossible to fully store energy through the PCM block in a short time and a large amount of PCM is left unused.

6.3. Nanofluid concentration

The purpose of this subsection is to analyze the effects of nanofluid concentrations on the energy storage capacity provided over a given period of time by calculating the liquid fraction in the PCM block. Fig. 15 shows the liquid fraction for Rayleigh numbers of 10^4 and 10^5 at fixed



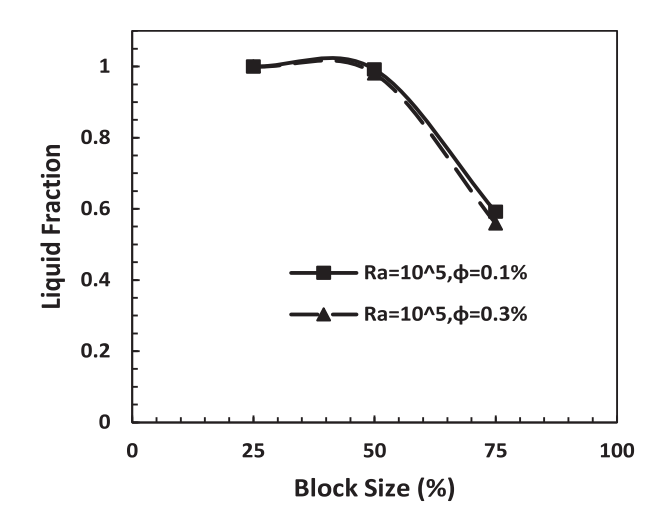


Fig. 15. Liquid fraction for $\phi = 0.1$ and 0.3%, pl = 0.01 and block size of 25,50 and 75% of radiation and natural convection at (a) $Ra = 10^4$ and (b) $Ra = 10^5$.

Planck number 0.01 for two nanofluid concentrations 0.1 % and 0.3 % at Fourier number of 0.38. The results are presented for three different sizes of PCM block 25, 50 and 75 %.

The liquid fraction is lower for the larger PCM block due to the blockage effect and lower heat transfer through the weak circulation of the nanofluid while increasing the amount of PCM. However, the surprising result is that for both Rayleigh numbers, the liquid fraction decreases with the increase in nanofluid concentration. From Fig. 15, increasing the nanofluid concentration from 0.1 % to 0.3 % reduced the liquid fraction up to 5.5 %. It is known that nanoparticles improve thermophysical properties in convection and conduction heat transfer. So, the reason for this observation should be found in the radiative properties of nanofluid, which increases the scattering and absorbing properties of radiation by nanoparticles in higher concentrations.

The change in these properties, including absorption and scattering, can be due to factors such as nanoparticle interactions that affect the radiation transfer. Therefore, it causes the radiative heat transfer through nanofluid to attenuate. The mathematical expression of this interpretation can also be seen in the source term of the energy equation. In this source term, $\beta(1\text{-}\omega)$ quantifies the radiative properties, and decreasing its value leads to a reduction in the effect of the radiative term in the energy equation. Decreasing heat radiation at nanofluid concentrations of 0.3 % reduces heat transfer to the PCM block and makes lower energy storage. As a result, for energy storage in the presence of nanofluids, the radiative properties of nanofluids are very important parameters that must be taken into account to achieve proper performance.

7. Conclusion

This study revealed a comprehensive numerical analysis of volumetric radiation and natural convection effects on phase change materials (PCMs) block located in nanofluids, employing a fully coupled Lattice Boltzmann Method (LBM) approach. The key findings are:

- 1. Volumetric radiation significantly enhances heat transfer, leading to faster PCM melting rates by >30 % and 50 % at Rayleigh numbers of 10^4 and 10^5 , respectively, and improved energy storage efficiency.
- 2. Reducing the Planck number from 1 to 0.01 leads to increase in contribution of volumetric radiation >90 %, significantly improving thermal performance.
- 3. Increasing the block size from 25 % to 75 % causes a blockage effect on the circulation, which results in reduced heat transfer to the right and bottom areas of the enclosure.

- 4. The increase in nanoparticle concentration from 0.1~% to 0.3~% leads to a slight decrease (<5.5 %) in the liquid fraction.
- The heat reduction by increasing nanofluid concentration is attributed to the increased scattering effects of the nanoparticles, which attenuate the radiative heat transfer.
- The LBM is a robust numerical approach for solving coupled volumetric radiation-natural convection-melting in thermal storage problems, offering accurate and beneficial results.

These findings provide crucial insights for designing PCM-nanofluid thermal storage systems, with applications such as solar energy storage, building heating and cooling, and thermal management devices. In order to validate the results of the present numerical method, future work can focus on experimental measurements. Simultaneous applications of Particle Image Velocimetry (PIV) and holographic interferometry to investigate the combined heat transfer inside the heated enclosure containing nanofluid and PCM block is suggested for the design of the experimental setup.

CRediT authorship contribution statement

Hashem Ahmadi Tighchi: Writing – original draft, Visualization, Validation, Methodology, Conceptualization. Masoud Sobhani: Writing – original draft, Validation, Methodology, Investigation. Javad Abolfazli Esfahani: Writing – review & editing, Supervision, Funding acquisition, Conceptualization.

Funding

This work is based upon research funded by Iran National Science Foundation (INSF) under project No. 4028093.

Declaration of competing interest

The authors declare the following financial interests/personal relationships which may be considered as potential competing interests: Javad Abolfazli Esfahani reports financial support was provided by Iran National Science Foundation (INSF). If there are other authors, they declare that they have no known competing financial interests or personal relationships that could have appeared to influence the work reported in this paper.

Data availability

Data will be made available on request.

References

- [1] Y. Zhao, X. Zhang, B. Yang, S. Cai, A review of battery thermal management systems using liquid cooling and pcm, J. Energy Storage 76 (2024) 109836.
- [2] T. Long, W. Li, Y. Lv, Y. Li, S. Liu, J. Lu, S. Huang, Y. Zhang, Benefits of integrating phase-change material with solar chimney and earth-to-air heat exchanger system for passive ventilation and cooling in summer, J. Energy Storage 48 (2022) 104037.
- [3] H. Behi, M. Ghanbarpour, M. Behi, Investigation of pcm-assisted heat pipe for electronic cooling, Appl. Therm. Eng. 127 (2017) 1132–1142.
- [4] F. Selimefendigil, H.F. Oztop, A.J. Chamkha, Natural convection in a cuo—water nanofluid filled cavity under the effect of an inclined magnetic field and phase change material (pcm) attached to its vertical wall, J. Therm. Anal. Calorim. 135 (2019) 1577–1594.
- [5] M. Boujelbene, H.S. Sultan, S. Mehryan, A.M. Hussin, A.S. Alghawli, M. Ghalambaz, Analyzing the melting process in a tilted heat sink filled with a phase change material equipped with the plate and optimized tree-shaped metal fins, J. Energy Storage 92 (2024) 111608.
- [6] H.F. Öztop, H. Coşanay, F. Selimefendigil, N. Abu-Hamdeh, Analysis of melting of phase change material block inserted to an open cavity, Int. Commun. Heat Mass Transf. 137 (2022) 106240.
- [7] H.F. Öztop, H. Coşanay, N. Biswas, F. Selimefendigil, Thermal energy storage via waste heat from finned heater by using different phase change materials in a closed space, J. Energy Storage 70 (2023) 108002.
- [8] N.S. Bondareva, M.A. Sheremet, A numerical study of heat performance of multipcm brick in a heat storage building, Mathematics 11 (2023) 2825.
- [9] M. Boujelbene, S.A. Mehryan, M. Sheremet, M. Shahabadi, N.B. Elbashir, M. Ghalambaz, Numerical study of a non-newtonian phase change flow in finned rectangular enclosures, Facta Univ. Ser.: Mech. Eng. 22 (2024) 1–24.
- [10] H.F. Öztop, H. Coşanay, N. Biswas, F. Selimefendiğil, Analysis of natural convection and melting in a separated cavity with nano-enhanced phase change material filled wall, Arab. J. Sci. Eng. (2023) 1–16.
- [11] A.A. Khan, A. Arshad, R. Ellahi, S.M. Sait, Heat transmission in darcy-forchheimer flow of sutterby nanofluid containing gyrotactic microorganisms, Int. J. Numer. Methods Heat Fluid Flow 33 (2023) 135–152.
- [12] Y. Yan, A. Safdari, K.C. Kim, Visualization of nanofluid flow field by adaptivenetwork-based fuzzy inference system (anfis) with cubic interpolation particle approach, J. Vis. 23 (2020) 259–267.
- [13] A. Zeeshan, R. Ellahi, M.A. Rafique, S.M. Sait, N. Shehzad, Parametric optimization of entropy generation in hybrid nanofluid in contracting/expanding channel by means of analysis of variance and response surface methodology, Inventions 9 (2024) 92.
- [14] R. Ellahi, The effects of mhd and temperature dependent viscosity on the flow of non-Newtonian nanofluid in a pipe: analytical solutions, Appl. Math. Model. 37 (2013) 1451–1467.
- [15] M. Bhatti, M. Arain, A. Zeeshan, R. Ellahi, M. Doranehgard, Swimming of gyrotactic microorganism in MHD Williamson nanofluid flow between rotating circular plates embedded in porous medium: application of thermal energy storage, J. Energy Storage 45 (2022) 103511.
- [16] P. Asinari, S.C. Mishra, R. Borchiellini, A lattice Boltzmann formulation for the analysis of radiative heat transfer problems in a participating medium, Numer. Heat Transf. B Fundam. 57 (2010) 126–146.
- [17] S.C. Mishra, R.R. Vernekar, Analysis of transport of collimated radiation in a participating media using the lattice Boltzmann method, J. Quant. Spectrosc. Radiat. Transf. 113 (2012) 2088–2099.
- [18] S.C. Mishra, H. Poonia, R.R. Vernekar, A.K. Das, Lattice Boltzmann method applied to radiative transport analysis in a planar participating medium, Heat Transfer Eng. 35 (2014) 1267–1278.
- [19] H. Ahmadi Tighchi, J. Esfahani, Combined radiation/natural convection in a participating medium using novel lattice Boltzmann method, J. Thermophys. Heat Transf. 31 (2017) 563–574.
- [20] H.A. Tighchi, M. Sobhani, J.A. Esfahani, Effect of volumetric radiation on natural convection in a cavity with a horizontal fin using the lattice Boltzmann method, Eur. Phys. J. Plus 133 (2018) 1–18.
- [21] M. Sobhani, H.A. Tighchi, J.A. Esfahani, Taguchi optimization of combined radiation/natural convection of participating medium in a cavity with a horizontal fin using LBM, Physica A Stat. Mech. Appl. 509 (2018) 1062–1079.
- [22] H.A. Tighchi, M. Sobhani, J.A. Esfahani, Lattice Boltzmann simulation of combined volumetric radiation/natural convection to consider optical properties of nanoparticles, Radiat. Phys. Chem. 159 (2019) 238–251.
- [23] M. Sobhani, H.A. Tighchi, J.A. Esfahani, Attenuation of radiative heat transfer in natural convection from a heated plate by scattering properties of Al₂O₃ nanofluid: LBM simulation, Int. J. Mech. Sci. 156 (2019) 250–260.
- [24] C. Wang, X. Liu, Y. Wei, K. Zhu, Y. Huang, Lattice Boltzmann scheme for coupled radiation–convection heat transfer in participating media, Phys. Fluids 35 (2023).
- [25] S. Souai, S. Trabelsi, E. Sediki, LBM simulation for combined thermal radiation and natural convection in 2D enclosure with multiple solid blocks, Numer. Heat Transf. A Appl. (2023) 1–26.
- [26] M. Izadi, A. Hajjar, H.M. Alshehri, M. Sheremet, A.M. Galal, Charging process of a partially heated trapezoidal thermal energy storage filled by nano-enhanced pcm using controlable uniform magnetic field, Int. Commun. Heat Mass Transf. 138 (2022) 106349.

- [27] Z. Said, R. Saidur, N. Rahim, Optical properties of metal oxides based nanofluids, Int. Commun. Heat Mass Transf. 59 (2014) 46–54.
- [28] B. Mondal, X. Li, Effect of volumetric radiation on natural convection in a square cavity using lattice Boltzmann method with non-uniform lattices, Int. J. Heat Mass Transf. 53 (2010) 4935–4948.
- [29] T. Yousefi, F. Veysi, E. Shojaeizadeh, S. Zinadini, An experimental investigation on the effect of Al₂O₃–H₂O nanofluid on the efficiency of flat-plate solar collectors, Renew. Energy 39 (2012) 293–298.
- [30] R. Saidur, T. Meng, Z. Said, M. Hasanuzzaman, A. Kamyar, Evaluation of the effect of nanofluid-based absorbers on direct solar collector, Int. J. Heat Mass Transf. 55 (2012) 5899–5907.
- [31] M.F. Modest, S. Mazumder, Radiative Heat Transfer, Academic press, 2021.
- [32] J.R. Howell, M.P. Mengüç, K. Daun, R. Siegel, Thermal Radiation Heat Transfer, CRC press, 2020.
- [33] M. Sheikholeslami, D. Ganji, Nanofluid convective heat transfer using semi analytical and numerical approaches: a review, J. Taiwan Inst. Chem. Eng. 65 (2016) 43–77.
- [34] A. Zeeshan, R. Ellahi, S.M. Sait, S. Nawaz Sharif, Heat transfer characteristics of hybrid nanoparticles in Newtonian fluid inside a channel with airfoil: a CFD simulation using comsol multiphysics, J. Comput. Appl. Mech. 56 (2025) 170–195.
- [35] X.-Q. Wang, A.S. Mujumdar, Heat transfer characteristics of nanofluids: a review, Int. J. Therm. Sci. 46 (2007) 1–19.
- [36] H.C. Brinkman, The viscosity of concentrated suspensions and solutions, J. Chem. Phys. 20 (1952) 571.
- [37] K. Khanafer, K. Vafai, M. Lightstone, Buoyancy-driven heat transfer enhancement in a two-dimensional enclosure utilizing nanofluids, Int. J. Heat Mass Transf. 46 (2003) 3639–3653.
- [38] P. Xu, M. Babanezhad, H. Yarmand, A. Marjani, Flow visualization and analysis of thermal distribution for the nanofluid by the integration of fuzzy c-means clustering ANFIS structure and CFD methods, J. Vis. 23 (2020) 97–110.
- [39] J. Heng, T. Thanapal, W.L. Chan, B. Elhadidi, Lattice Boltzmann simulation on the flow behaviour associated with Helmholtz cavity-backed acoustic liners, J. Vis. 23 (2020) 625–633.
- [40] A. Mohamad, Lattice Boltzmann Method vol. 70, Springer, 2011.
- [41] N. Jiang, E. Tian, N. Nabipour, A. Safdari, Visualization of dispersed phase in the carrier phase with lattice Boltzmann method through high-and low-resolution observations, J. Vis. 23 (2020) 377–381.
- [42] P.L. Bhatnagar, E.P. Gross, M. Krook, A model for collision processes in gases. I. Small amplitude processes in charged and neutral one-component systems, Phys. Rev. 94 (1954) 511.
- [43] T. Krüger, H. Kusumaatmaja, A. Kuzmin, O. Shardt, G. Silva, E.M. Viggen, The lattice Boltzmann method 10, Springer International Publishing, 2017, pp. 4–15.
- [44] B. Mondal, S.C. Mishra, Simulation of natural convection in the presence of volumetric radiation using the lattice Boltzmann method, Numer. Heat Transf. A Appl. 55 (2008) 18–41.
- [45] H. Dixit, V. Babu, Simulation of high rayleigh number natural convection in a square cavity using the lattice Boltzmann method, Int. J. Heat Mass Transf. 49 (2006) 727–739.
- [46] W. Miller, S. Succi, A lattice Boltzmann model for anisotropic crystal growth from melt, J. Stat. Phys. 107 (2002) 173–186.
- [47] I. Rasin, W. Miller, S. Succi, Phase-field lattice kinetic scheme for the numerical simulation of dendritic growth, Phys. Rev. E Stat. Nonlin. Soft Matter Phys. 72 (2005) 066705.
- [48] W.-S. Jiaung, J.-R. Ho, C.-P. Kuo, Lattice Boltzmann method for the heat conduction problem with phase change, Numer. Heat Transf. B Fundam. 39 (2001) 167–187
- [49] D. Chatterjee, S. Chakraborty, An enthalpy-based lattice Boltzmann model for diffusion dominated solid–liquid phase transformation, Phys. Lett. A 341 (2005) 320–330.
- [50] R. Samanta, H. Chattopadhyay, C. Guha, A review on the application of lattice Boltzmann method for melting and solidification problems, Comput. Mater. Sci. 206 (2022) 111288.
- [51] C. Huber, A. Parmigiani, B. Chopard, M. Manga, O. Bachmann, Lattice Boltzmann model for melting with natural convection, Int. J. Heat Fluid Flow 29 (2008) 1469–1480.
- [52] M. Seddiq, M. Maerefat, M. Mirzaei, Modeling of heat transfer at the fluid-solid interface by lattice Boltzmann method, Int. J. Therm. Sci. 75 (2014) 28–35.
- [53] F. Moufekkir, M. Moussaoui, A. Mezrhab, H. Naji, D. Lemonnier, Numerical prediction of heat transfer by natural convection and radiation in an enclosure filled with an isotropic scattering medium, J. Quant. Spectrosc. Radiat. Transf. 113 (2012) 1689–1704.
- [54] F.-H. Lai, Y.-T. Yang, Lattice Boltzmann simulation of natural convection heat transfer of Al₂O₃/water nanofluids in a square enclosure, Int. J. Therm. Sci. 50 (2011) 1930–1941.
- [55] M. Paroncini, F. Corvaro, Natural convection in a square enclosure with a hot source, Int. J. Therm. Sci. 48 (2009) 1683–1695.
- [56] K.A. Rathjen, L.M. Jiji, Heat Conduction With Melting or Freezing in a Corner, 1971.
- [57] D. Li, Z.-X. Tong, Q. Ren, Y.-L. He, W.-Q. Tao, Three–dimensional lattice Boltzmann models for solid–liquid phase change, Int. J. Heat Mass Transf. 115 (2017) 1334–1347.